DIFFUSED CORRELATION SPECTROSCOPY FOR MEASUEREMENT OF BLOOD PERFUSION DURING LOW LEVEL LASER THERAPY (LLLT)

by

SAGAR SUNIL SONI

Presented to the Faculty of the Graduate School of

The University of Texas at Arlington in Partial Fulfillment

of the Requirements

for the Degree of

MASTER OF SCIENCE IN BIOMEDICAL ENGINEERING

THE UNIVERSITY OF TEXAS AT ARLINGTON

MAY 2016

Acknowledgements

I would like to express my gratitude to Dr. Hanli Liu for offering me a chance to work on her vision and having faith in me throughout. She has been extremely supportive, understanding and has encouraged me to become an independent learner. I am very grateful for all the resources and knowledge that I gained during the course of my masters from Dr. Liu. I am extremely inspired by her and her work.

I am extremely thankful to Dr. George Alexandrakis, Dr. Michel Nelson and Dr. Liu for being on my thesis defense committee despite their busy schedules and offering me their valuable advice.

I would like to express my gratitude to Dr. Tian Fenghua for mentoring me and being extremely patient with my pace of learning throughout the course of this project. I appreciate all his contributions of time, ideas and advices during the entire course of the project. I would also like to express my gratitude to all my lab-mates who helped me at various stages of the project.

I want to thank all my friends who have encouraged, advised and cheered me up all the way through. Finally, I would like to thank my parents Mr. Sunil Soni, Mrs. Kiran Soni, my brother Mr. Suraj Soni and my sister-in-law Mansi Soni for their blessing, and encouraging and believing in me throughout my life.

April 27th, 2016

Abstract

DIFFUSED CORREALTION SPECTROSCOPY FOR MEASUREMENT OF TISSUE BLOOD PERSUION DURING LOW LEVEL LASER THERAPY (LLLT)

Sagar Sunil Soni, M.S.

The University of Texas at Arlington, 2016

Supervising professor: Dr. Hanli Liu

Near infrared stimulation or Low Level Laser Therapy (LLLT) is an innovative technique shown to effect the microvasculature hemodynamics. The aim of this study is to use Diffused Correlation Spectroscopy (DCS) to evaluate the physiological effects of LLLT on blood perfusion. This study is divided into two parts: the fist part is the development of DCS system and the second part is investigating the effects of LLLT on biological tissue.

DCS is an emerging non-invasive technique to probe deep tissue hemodynamics. DCS uses time-averaged intensity autocorrelation function for the fluctuations caused due to the moving scatterers (RBCs) in biological tissue. We present a software based autocorrelator system to complete the acquisition and processing parts. We conducted validation studies on an intralipid phantom and human forearm. Both the studies proved smooth decay curves which help in getting a better curve fitting and as a result more accurate blood flow index (BFI). We show that the software based autocorrelation system can be an alternative to the conventional hardware

based correlators in DCS systems with benefits such as flexibility in raw photon count data processing and low cost.

The objective of the second part of this study is evaluating how a single session of LLLT alters the hemodynamics in the microvasculature. We performed an experiment where the subjects forearm was stimulated with LLLT and the corresponding changes were recorded using DCS system. The results obtained shows significant hemodynamic changes in response to LLLT with a 95%confidence interval. The results in this study indicate that LLLT could lead to the development of non-invasive technique to help in rehabilitation and performance-enhancing of healthy humans.

Table of Contents

List of Illustrations

List of Tables

Chapter 1

Introduction

1.1 Diffused Correlation Spectroscopy

Light is an excellent tool which could be used to probe human tissue. It has the potential to non-invasively acquire information about tissue optical and dynamic properties, thus offering exciting possibilities in the field of medical imaging [1]. Models for light propagation in the late 1980s have paved the way for large variety of applications. Diffuse optics has opened up new possibilities for non-invasive medical devices for diagnosis of lesions in deep tissue. In addition, the usage of light makes optics-based medical devices compatible with other conventional devices such as CT and MRI as well as implanted device such as pacemaker. Diffuse optics-based devices are also relatively cost-effective and portable. These merits extend the applications of such medical devices to primary care unit, bedside monitoring, and operation theater as an optical modality for probing hemodynamic properties in the microvasculature of deep tissue [2].

Diffused Correlation Spectroscopy (DCS) is an emerging non-invasive technique to probe the deep tissue blood perfusion, by using time-averaged intensity autocorrelation function of the fluctuating diffuse reflectance signal. DCS technology has been extensively developed, validated and employed in the last decade to probe the blood perfusion information in the deep tissue vasculature, such as brain, muscle and breast [3].

1.1.1 Optical Window

The propagation of light through tissues is complicated by the properties of scattering and absorption of the incident light. Optical absorption in biological tissues is primarily due to the pre-

resence of hemoglobin, melanin and water (see figure 1) [4]. In the late 1970s, Jobsis [5] realized that there exits a "window" in the near-infrared spectrum (NIR) where the photons could travel deep into the tissue because of the reduced absorption of incident light due to water (refer figure 1). DCS operates in this window where there is very low absorption of light by the biological tissue which enables deep penetration of light [3].

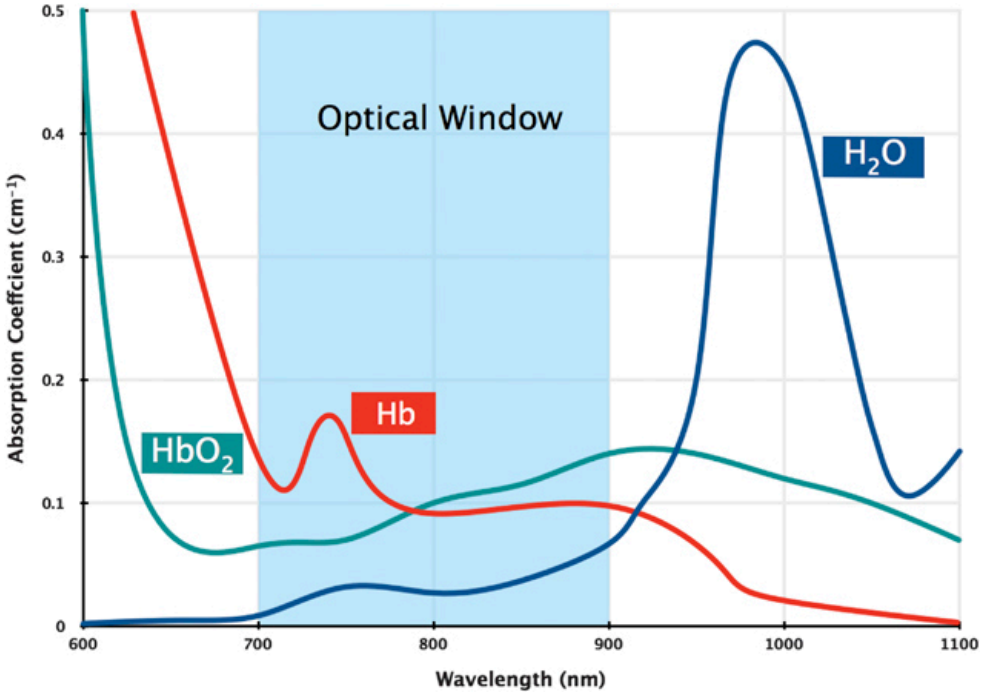

Figure 1: Absorption Spectrum of Hb, HbO2 and water invisible and near-infrared range [6]

The lower wavelengths such as violet and ultraviolet have poor tissue penetration due to the increased absorption of light by the blood and tissue components [7]. Similarly water significantly absorbs the light higher than 1000nm. In between these wavelengths the penetration of light is higher due to low absorption. This region (~650nm - 1100nm) is termed as optical window for non-invasive optical imaging (refer figure 1). In this window, scattering is the dominant interaction which takes place in the tissue. The light diffuses into the tissue due to this scattering and light is able to propagate through the tissue thickness of ~15 cm for limbs, brain and breast [8]. Thus this

NIR optical window is ideal range for non-invasive study of hemodynamics of microvasculature in tissue.

1.1.2 Diffusion of light in blood

Photons which enter the tissue undergo two types of interactions with the tissue: (1) absorption, which may lead to radiation-less loss of energy, or induce fluorescence or phosphorescence, and (2) scattering, which may or may not change the frequency and induce a phase shift by scattering off of moving particles in the tissue (for example, blood cells) [9]. Out of these two interactions scattering is more dominant and as a result a tissues are considered a scattering or turbid media [4]. Due to this interaction the trajectory of the diffused light is also changed (See Figure 2).

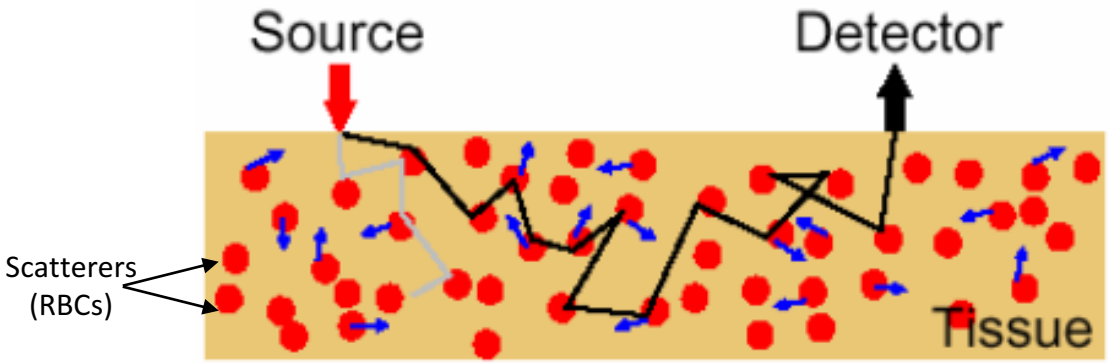

Figure 2: Diffusion of light in biological tissue [27]

DCS is an extension of single-scattering dynamic light scattering (DLS) [29-31] to multiple scattering limit. When light photons are diffused in the tissue, they may experience phase shifts and cause speckle fluctuations at the detector side. The motion information of the scatter is carried by the electric field of the attenuated light and can be obtained from the electric field autocorrelation function [3]. This function if defined as:

$$G(\vec{r}, \tau) = \langle E(\vec{r},t)\, E^*(\vec{r},t+\tau) \rangle \quad 1.1$$

Experimentally, the diffuse autocorrelation equation is calculated as:

$$g(\vec{r}, \tau) = \frac{\langle E(\vec{r},\tau) E*(\vec{r},t+\tau)\rangle}{\langle I\rangle^2} \quad 1.2$$

Siegert proved that the phase information is retained. Equation 3 is calculated using this Siegert Relation: [3,11]

$$g(\vec{r}, \tau) = 1 + \beta \frac{|G(\vec{r},\tau)|}{\langle I(\vec{r},t)\rangle^2} \quad 1.3$$

Where I ($\vec{r}$,t) is the detected diffusing light intensity at position r and time t, the angle bracket ⟨…⟩ denotes an ensemble average, and β here is a numerical factor related to the detector geometry, number of detected speckles and other experimental parameters [3]. The Siegert relation is used to obtain the electric field autocorrelation function with the assumption that the systems' time average is equal to ensemble average [3]. Studies have showed that, although the movement of RBCs is considered as a random motion, The Brownian motion model showed better fitting in the majority of the cases ranging from muscle to brain and also tumor models. Thus G_1 ($\vec{r}$,) can be fitted to parameterize relative blood flow[3] .

1.2 Low Level Laser/Light Therapy (LLLT)

Light is a form of electromagnetic (EM) which may be visible or invisible to the human eye. EM waves are described by their frequency and wavelength which helps to categorize them into different spectrums which include radio waves, microwaves, infrared radiation, visible light, ultraviolet light, x-rays and gamma rays based on their wavelength in the descending order. Infrared radiation ranges from nominal red edge of the visible spectrum at 700nm to 1mm. Non-thermal near infrared spectrum ranges from 700nm to 2000nm wavelength. As discussed on 1.1.1, near-infrared wavelength is highly permeable in biological tissue and can be used for therapeutic applications.

Low Level Laser Stimulation (LLLT) can be defined as the use of bidirectional low-power and high-fluence monochromatic or quazimonochromatic light from lasers or light-emitting diode (LEDs) in the red to near-infrared wavelengths (λ = 600nm – 1100nm) to modulate a biological function or induce a therapeutic effect in a non-destructive and non-thermal manner [11]. The principle behind LLLT is based on the law of conservation of energy. The luminous energy is converted to metabolic energy with a subsequent modulation of the biological functioning of the cells. This indicates that the molecules stimulated by light acquire an excited state which temporarily changes its configuration and function. As a result, LLLT is also known as photobiomodulation [11].

1.2.1 Properties of LLLT Source

Unlike Solar energy LLLT is monochromatic and allows for high specificity and targeted molecular biomodulation. Many applications of lasers in LLLT are characterized by destructive effects of energy over discrete areas of tissues. This is because lasers deliver concentrated energy

which are highly monochromatic, unidirectional and coherent. Lasers allow deep tissue penetration and the radiation can be controlled as they produce a constant bean width which offers the advantage of energy delivery on bounded areas. Thus the advantages of laser sources include high monochromaticity, efficient fiber optic coupling which can be used to modify beam width and deep tissue perpetration [11]. LED sources can produce a narrow band of wavelengths in the range of 4nm to 10 nm and are non-coherent. This property of no coherence of LEDs is the reason there is significant difference in the amount of energy delivered to single targeted area. Some advantages of LEDs over lasers is that they produce no or negligible amount of heat which reduces the risk of injury. LEDs and solid state lasers are compact and portable which is ideal in the case of clinical setting. LEDs can be mounted in arrays to improve ergonomics and better energy delivery [11].

Some important parameters to consider while performing LLLT are listed in Table 1 below

Table 1: Parameters of LLLT [11]

Light source	Wavelength	Dose	Effect	Relevance	Reference
He-Ne laser	632.8 nm	10.5 mW, 1.1 mm beam diameter × 2 minutes, daily for 2 weeks	Preserved structure and function after optic nerve crushed injury (rat, rabbit)	Optic nerve trauma	Schwartz et al,[71] Assia et al,[72]
GaAlAs LED	670 nm	28 mW/cm^2, 12 J/cm^2 in three fractions	Preserved structure and function after systemic methanol photoreceptor toxicity (rat)	Methanol intoxication	Eells et al,[12]
GaAlAs LED	633 nm	2 mW/cm^2, 21.6 J/cm^2 in six fractions	Preserved structure and function after intravitreal rotenone injection (rat)	Leber's hereditary optic neuropathy	Rojas et al,[49]
GaAlAs LED	670 nm	16 J/cm^2 in four fractions	Preserved structure and function after laser retinal photocoagulation (monkey)	Laser-induced retinal injury	Eells et al,[76]
GaAlAs LED	670 nm	50 mW/cm^2, 20 J/cm^2 in five fractions	Preserved structure in the P23H-3 rat (rat)	Retinitis pigmentosa	Eells et al,[76]
GaAlAs LED	670 nm	50 mW/cm^2, 360 J/cm^2 in four fractions	Preserved structure and function after phototoxicity (rat)	Light-induced retinal damage	Qu et al,[73]
ILPD	904 nm	4500 mW/cm^2, 45,000 J/m2, pulsed at 3 MHz	Improved function in an 86-year-old man with macular degeneration (human)	Age-related macular degeneration	Rodriguez-Santana et al,[77]

Abbreviations: GaAlAs LED, Gallium-Aluminum-Arsenide light-emitting diode; He-Ne, Helium-Neon; IPLD, intense pulsed light device.

1.2.2 Targets for Low Level Laser/Light Therapy (LLLT)

Light uptake in a biological cell is based on the presence of biomolecules that have the property to be excited by light. These molecules are known as biomolecules. There are two main types of biomolecules: (1) Those which include photo pigment molecules such as chlorophyll in plants, and rods and cones in in the human retina. These specialized molecules are called photoreceptors. (2) the non-specialized molecules that can absorb light but are not integral to light receptor organs are called photoacceptors. These photoacceptors, although not directly related with light processing, are usually part of metabolic pathways. The theory of LLLT photobiology is based on the mechanism of the action due to modulation of photoacceptor function [11]. Another important concept is that of a chromophore. A chromophore is similar to both photoreceptor and photoacceptor. Chromophores are usually metal ions or organic cofactors within a protein structure and contain electrons which could be excited from ground to excited state [11].

Incidence of light on the chromophore caused its electron to jump from lower energy orbit to higher energy orbit. This excitation can be stored in the cell to perform cellular tasks. This excitation caused cellular changes in the shape of the molecule which is related to functional and intracellular metabolism [12]. In cells, the chromophores can consist of metal complex or resonating systems. In metal complexes, electron excitation occurs in open or closed pyrole rings that allow binding of transition metals. Alternatively, in resonating systems the electron excitation by light occurs within a structure which alternates the single and double bonds [11].

It has been proved that in LLLT the mitochondria are responsible for cellular response of red visible and NIR light. Mitochondria are known as the "powerhouse" of the cell as they are responsible for cellular respiration where food is converted into energy in the form of ATP via the process of oxidative phosphorhylation. A eukaryotic cell typically has about 2000 mitochondria.

A dominant role of mitochondria is production of ATP by oxidizing the major products of glycolysis, pyruvate and NADH that are produced in the cytosol [14]. The basic principle behind production of ATP is a three-step process. In the first step pyruvate molecule is produced by the process of glycolysis. The second step, each pyruvate molecule is oxidized and combined with coenzyme A to form CO_2, acetyl-CoA and NADH. The acetyl-CoA is the primary substrate to enter the citric cycle, also known as tricarboxylic acid (TCA) cycle or Krebs cycle. The TCA cycle oxidizes the acetyl-CoA to CO2 and produces cofactors which are three molecules of NADH and one molecule of FADH2 . These cofactors are the source of electrons for the electron transport system (ETS) and a molecule of GTP. GTP can readily be converted to ATP [blood LLLT]. High energy electrons pass through the ETS to the final acceptor generating a proton gradient which is used by the enzyme ATP synthase to produce ATP. Figure 4 shows the illustration of a mitochondria and the electron transport chain and oxidative metabolism.

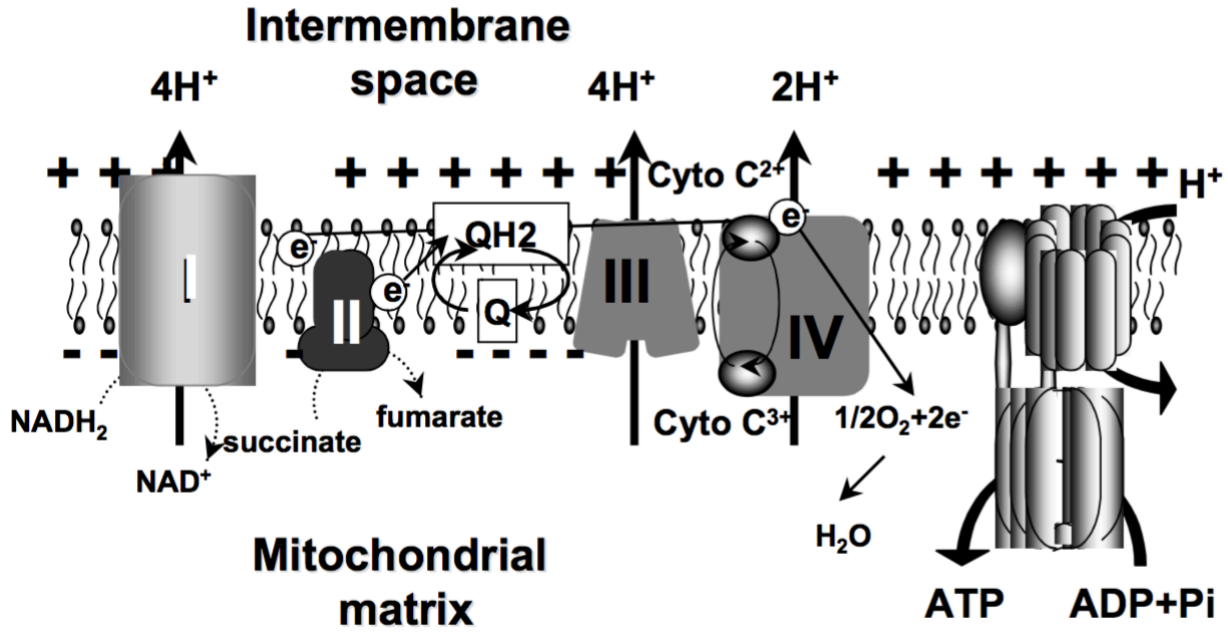

Figure 3: Electron Transport Chain in mitochondrial inner membrane [14].

The enzyme cytochrome C oxidase (CCO), which is one of the four membrane bound complexes which is embedded in the inner membrane of the mitochondria, is an effective energy converting unit as it generates a electrochemical gradient through redox reactions and also is a rate limiting step required for the formation of ATP [13].

Each CCO is a multicomponent protein complex. It contains two iron cores, haem a and haem a_3 and two copper cores, Cu_A and Cu_B [14]. (See Figure 5) These metal cores decide the different light absorption peaks for CCO: Cu_A is reduced at 620nm (range 613.5-623.5nm), and Cu_A oxidizes at 825nm (range 812.5-845nm), Cu_B reduction and oxidation is at 760 nm (range 750.7-772.3nm) and 680nm (range 667.5-683.7nm) respectively [14].

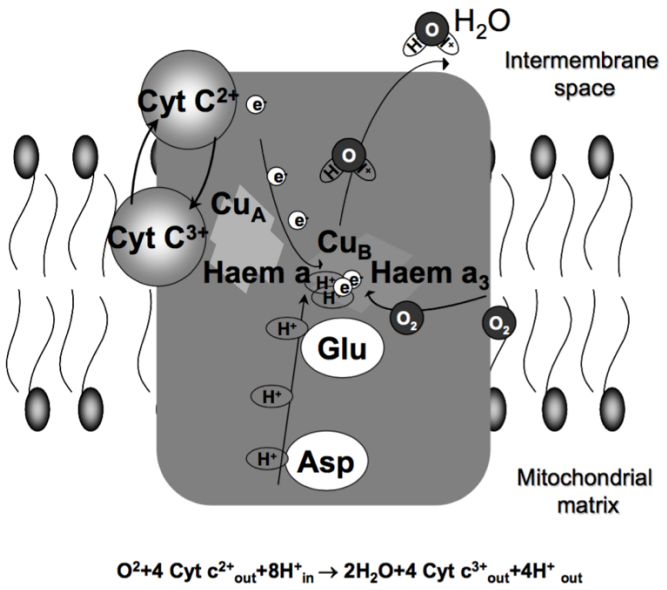

Figure 4: Structure and mode of action of cytochrome c oxidase [15]

1.2.3 Mechanism of Action of LLLT

It is clear now that cytochrome oxidase it the primary photoacceptor of LLLT. The effects of LLLT could be divided into two effects: (1) Primary effect during light exposure and (2) Secondary effects after light exposure [11].

1.2.3.1 Primary Effects

The Primary effects of LLLT are the direct photochemical changes which occur in the photoreceptor upon excitation due to light. There are three primary effects due to the light-dependence. The first is the redox change of the components in the respiratory including the reduction or oxidation of cytochrome oxidase. These changes implicate the alterations in the electron flow. LLLT increases cytochrome c oxidation in the presence of cytochrome oxidase, which increases the oxygen consumption and mitochondrial membrane potential and it activates the membrane pore of the mitochondria [11].

The second likely effect is the generation of free radicals, which include singlet oxygen via direct photodynamic action and superoxide ion via one electron auto oxidation. The reactive oxygen species not only damage the by-products of respiration but also have an important role in cellular signaling.

The third primary effect is the localized transient heating of absorbing chromophore because of the incident light oscillations [15]. This effect has been less characterized and it is believed to complement the other two primary effects of LLLT. This effects seem to affect all the molecules in the target tissue, including water molecules. LLLT strengthens the hydrogen bonds and large size bond networks which allow rapid energy transfers due to resonant intermolecular energy transference. As a result, LLLT can cause nonequillibrium fluctuations in which bias Brownian movement and induce mechanisms that support electron pumping without heat transfer [16].

1.2.3.2 Secondary effects

The secondary effects are light independent effects and occur as a result of the primary effects. The secondary effects are a series of equations which change the cellular homeostasis [11,

17, 18]. Secondary effects feature activation of second messengers with subsequent modulation of enzyme function and gene expression. Secondary effects are unique as they can occur hours and even days after light exposure and they associate the activation of signaling pathways which result in the amplified macro effects. LLLT triggers the signaling pathway from mitochondria to the nucleus which causes the adaptive responses to stress by sending information from mitochondria to the nucleus, which can respond to gene expression [11]. The initial phase of the signaling pathway has been suggested to be an increase in the NAD / NADH ratio, the intermembrane potential on the mitochondria, dissociation of nitric oxide (NO) from cytochrome oxidase, and modification of ATP pool. Even small changes in ATP alters the cellular metabolism. ATP activates the P2 receptor (P2X and P2Y) to induce inward calcium currents and release calcium for intracellular stores and the formation of cyclic adenosine monophosphate (cAMP) [18]. Changes in the ATP levels alter the cyclic adenosine monophosphate levels, with consequent activation of kinases. Depending on the cell environment, these cellular changes can be adaptive and promote enhancement of neuronal physiology which results in clinical improvement [11].

1.2.4 Effect of LLLT on blood perfusion

In the secondary effects of LLT on mitochondria, nitric oxide (NO) is photodissociated from cytochrome oxidase. NO is a free radical gas which is a powerful regulator of blood circulation as it is an endogenous vasodilator. NO closely resembles O_2 and therefore can also bind to the copper centers in CCO and inhibit respiration. It has been proposed that LLLT might work by photo-dissociating NO from the cytochrome c oxidase, thereby reversing the signaling consequences of NO binding [14]. Vasodilation caused my LLLT was first described in 1968 by R. F. Furchgott, in his nitric oxide research which lead to a Nobel Prize in 1998 [19]. Later studies

extended Furchgott's early work and demonstrated the the ability of light to influence localized production or release of NO and cause vasodilation [14]. But the wavelengths corresponding to the light mediated release of NO are different form LLLT range being in the blue and ultraviolet range.

Some wavelengths of light are absorbed my hemoglobin which releases NO from hemoglobin from nitrosothils in the beta chain of the hemoglobin molecule in RBCs [20-22]. As the RBCs are delivered continuously to the area of treatment, there is a natural supply of NO. This release of NO is highly local since the half life of NO is 2 to 3 seconds. The wavelength which correspond to this phenomenon tend to be in the in the UVA rand blue range not same as that for LLLT [23].

Tiina Karu provided the evidence that NO was involved in the response of the cell to LLLT in the red spectrum region [24]. Other in vivo studies on the use of 780 nm and 804nm laser for stimulating bone healing in rates [25] and to decrease the damage inflicted in rat hearts after creation of heart attacks [26] respectively, has shown significant increase of NO in illuminated tissues after LLLT. However, studies carried out with read and NIR light sources have both shown reduction of NO in tissues. The authors explained this phenomenon by suggesting LLLT inhibited iNOS [14].

Many studies describe increased blood flow in animal models and in patients during and after LLLT. However, it is still not clear whether blood flow arise from LLLT is mediated by the the release of NO [14]. The increase in the blood flow could be due to the production of CO_2 in the TCA cycle. Carbon dioxide has a profound effect on blood flow. Several mechanisms involved in hypercapnic vasodilation due to increased CO_2, the major mechanism appears to be related to a direct effect of extracellular H^+ on vascular smooth muscles [27].

1.3 Focus of this Study

Low level laser/light therapy (LLLT) consists of applying highly focused monochromatic light in the "optical window" to biological tissue in the red to near infrared (NIR) region. LLLT has gained attention in the recent decade as a novel method for applications in therapeutic medicine.

The first part of the study is developing a Diffused Correlation Spectroscopy system to monitor blood perfusion in biological tissue. DCS is an emerging technique to non-invasively monitor blood flow and blood perfusion. We present a novel DCS system with a software based autocorrelation system using National Instruments' LabVIEW and Mathworks' MATLAB. This system inherits the attractive properties such as non-invasiveness, high penetration depth, high temporal resolution along with some unique properties such as ability to process raw photon count and save the data in any required format along with being low cost when compared to a hardware-based correlator.

The second part of this study deals with understanding the physiological effects of Low Level Light/Laser Therapy (LLLT) in microvasculature in biological tissue. Most of the studies evaluated the theory behind the increased blood flow in biological tissue due to LLLT. No study has been done to monitor the blood perfusion change before, during and after LLLT using DCS system. This study is aimed at understanding the physiological changes which occur in the cell which produce a change in blood perfusion to the treated area of tissue. The hemodynamic response of the tissue is associated with the activation of cytochrome c oxidase in the mitochondrion due to LLLT.

1.4 Outline of this Thesis

Chapter 1 gives a brief introduction about the basic principle of DCS system and Low Level Light/Laser Therapy (LLLT). Chapter 2 deals with the instrumentation of Diffused Correlation Spectroscopy (DCS) system. This chapter contains the theoretical background of DCS, Data analysis and methodology along with the verification and validation of the system. Chapter 3 examines the physiological effects of LLLT on microvascular blood perfusion on biological tissue. It has description of subjects, protocol and data analysis and results obtained from the experiment. Chapter 4 discusses the obtained results. It also discusses the limitations and the future work of the study.

Chapter 2

Diffused Correlation Spectroscopy

Measurement of microvascular blood flow (BF) holds key to useful information for diagnosis of tissue disease and for monitoring therapeutic effects. Microvascular BF delivers nutrients such as oxygen to tissue and removes metabolic waste products from tissue. Abnormal BF is related to cardiovascular disease stroke, head trauma, peripheral vascular disease (PVD), cancer. The ideal technique for measurement of BF provides quantitative information about micro and macro-vasculature with ability of probe deep tissues. [32]. Near-infrared Diffused Correlation Spectroscopy (DCS) also known as diffusing-wave spectroscopy (DWS) is established as an emerging technique for continuous non-invasive measurement of blood perfusion in biomedical tissues. Compared to other modalities for monitoring tissue blood flow, such as positron emission tomography (PET), single photon emission computed tomography (SPECT), and xenon-enhanced computed tomography (XeCT), DCS uses non-ionizing radiation and has no need of a contrast agent. Also DCS is safe to use with other medical devices such as metal implants and pacemakers [3].

NIR diffused optical spectroscopies are separated into “static” and “dynamic” methods to probe the motions of the scatterers. NIRS is a “static” method since it measures the relatively slow variations in tissue absorption and scattering. “Dynamic” methods directly measure the motions of the scatterers. In terms of biological tissue, the RBCs are the primary moving scatterers. The detected signal from biological tissue is related to the motion of the RBCs, BF can be derived using a mathematical model of the propagation of light photon through tissue [32].

2.1 Fundamentals of Diffused Correlation Spectroscopy

As discussed in 1.1.2, DCS is πππan extension of single-scattering dynamic light scattering (DLS) extended to multiple scattering limit for the study of optically thick samples. In this section we discuss the single-scattering theory, and then extend it to multiple scattering limit.

2.1.1 Single Scattering

In a single-scattering experiment, photons are usually scattered only once or not at all. In the simplified experiment setup (See Figure 2.1) a point-like photon detector is placed at an angle θ relative to the input beam direction. If the scatterers move, the total electric field will vary in time. At the detector, the scattered electric field from the i^{th} particle is

$$\begin{aligned} \mathbf{E_i}(t) &= \hat{\mathbf{e}} E_0 F(\theta) e^{-i\omega t} e^{i\mathbf{k_{in}}\cdot[\mathbf{r_i}(t)-\mathbf{R_s}]+i\mathbf{k_{out}}\cdot[\mathbf{R_d}-\mathbf{r_i}(t)]} \\ &= \hat{\mathbf{e}} E_0 F(\theta) e^{-i\omega t} e^{i(\mathbf{k_{out}}\cdot\mathbf{R_d}-\mathbf{k_{in}}\cdot\mathbf{R_s})} e^{-i\mathbf{q}\cdot\mathbf{r_i}(t)}, \end{aligned} \quad 2.1$$

Where $\hat{e}$ is a unit vector indicating the polarization direction of the scattered field. E_0 is the amplitude of the incident field, F(θ) is the scattering form factor which depends on the particle size, shape, refraction index and scattering angle θ. ω is the angular velocity of light. Since we are using a long coherence length CW laser, we assume the light source is monochromatic. k_{in} and k_{out} are the input ad output wave vectors, $k_0 = |k_{in}| = |k_{out}| = \frac{2\pi n}{\lambda}$. n is the index of refraction, λ is the wavelength of the incident light, $q = k_{out} - k_{in}$ is the momentum transfer for the scattering geometry; $|q| = 2k_0\sin(\theta/2)$. R_d, R_s and r_i indicate the positions of the detector, source and scatterer respectively. The total scattered eclectic field at the detector is given by:

$$\mathbf{E_T}(t) = \sum_{i=1}^{N} \mathbf{E_i}(t) = \hat{\mathbf{e}} E_0 F(\theta) e^{-i\omega t} e^{i(\mathbf{k_{out}}\cdot\mathbf{R_d}-\mathbf{k_{in}}\cdot\mathbf{R_s})} \left(\sum_{i=1}^{N} e^{-i\mathbf{q}\cdot\mathbf{r_i}(t)} \right) \quad 2.2$$

Where the summation is over all N scatterers in the beam.

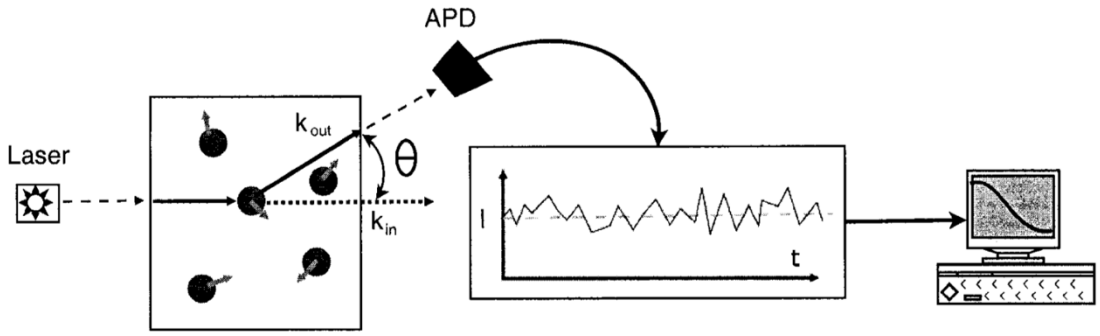

Figure 5: Illustration of diffused optical tomography [33]

If the scatterers are static, then the total electric field at the detector is constant. However, if the scatterers are in motion, the total electric field is a function of time. Thus by understanding the fluctuations in the electric field at the detector, the properties of the medium can be determined. To quantify this, we calculate the unnormalized autocorrelation function of the total scattered electric field [33].

$$G_1(\tau) = \langle E(t)\, E^*(t+\tau) \rangle \qquad 2.3$$

Here, τ is the autocorrelation lag time and $\langle \triangle r^2(\tau) \rangle$ is the mean square displacement of the scatterers in the medium in the time delay τ. In most of the experiments, the normalized intensity autocorrelation function

$$g_2(\tau) = \langle I(t)I(t+\tau) \rangle / \langle I(t) \rangle^2 \qquad 2.4$$

is calculated from the intensity fluctuations in the scattered light. $G_2(\tau)$ is related to $g_1(\tau)$ by the Siegert relationship.

$$g2(\tau) = 1 + \beta \frac{|G(\vec{r},\tau)|}{\langle I(\vec{r},t)\rangle^2} \quad 2.5$$

Here, the term β depends on the detection optics and is inversely proportional to the number of detected speckles. β can be determined experimentally for each measurement from the intercept of the intensity autocorrelation function as the delay time τ approaches zero [32,33].

2.1.2 Multiple Scattering Limit (DWS)

Multiple scattering is must be included in the case of biomedical tissues since the concentration of particles is increased and the light photos are scattered many times before they exit the tissue. The moving scatterers in the biomedical tissue contributes to the accumulation of the phase shift which leads to the decay of correlation function. Figure 6 shows the schematic representation of multi-scattering setup showing photon path through turbid media. The total temporal field autocorrelation function can be expressed as:

$$g_1(tau) = e^{iw\tau} e^{\frac{-1}{3}k_0^2 Y\langle \Delta r^2(\tau)\rangle} \quad 2.6$$

Where Y = N.(1-$\langle\cos\theta\rangle_N$ and $\langle\cos\theta\rangle_N$ is the average of the cosine over all the N scattering events along the path. When the number of scatterers are very large, the average value of approaches ensemble average, $\langle\cos\theta\rangle$, which is denoted by anisotropy factor (g) of the medium [32]. The reduced scattering length or random walk step length is given by $l_s^* = 1/ \mu_s'$. The number if scattering events associated with the same path is $N = s/l_s$ where s is the total pathlenght associated with a particular path, and $Y = s/l_s^*$ equals the total number of photon random walk steps associated with the photon path length [33].

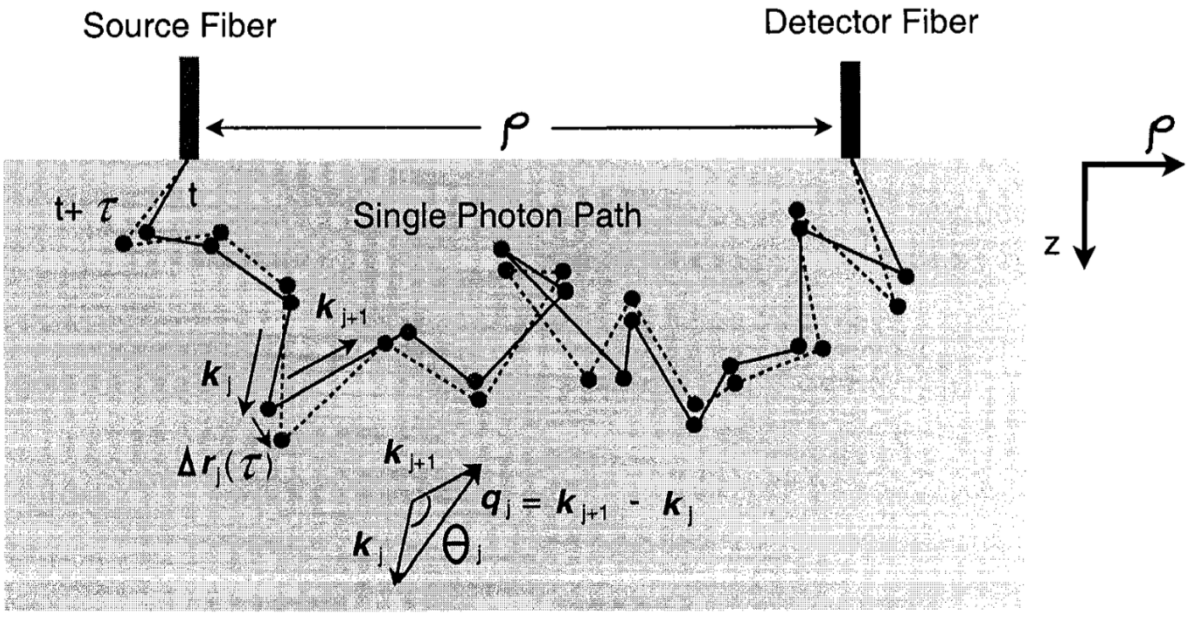

Figure 6: Illustration of dynamic light scattering experiment [33]

The total electric field autocorrelation function contains the contribution of all photons paths. The total electric autocorrelation function can be computed by integrating the contributions from each photon path i.e.

$$g_1(\tau) = e^{iw\tau} \int_0^\infty P(Y)\, e^{\frac{-1}{3}k_0^2 Y\langle \Delta r^2(\tau)\rangle} \mathrm{dy} \qquad 2.7$$

where P(Y) represents the probability distribution for photon paths with number of random walk steps Y. In highly scattering medium equation 2.7 can be expressed as an integral over all possible pathlengths.

$$g_1(\tau) = e^{iw\tau} \int_0^\infty P(s)\, e^{\frac{-s}{3ls*}k_0^2 Y\langle \Delta r^2(\tau)\rangle} \mathrm{ds} \qquad 2.8$$

Equation 2.8 is the primary result of DWS for a homogeneous turbid scattering medium composed

of moving particle-like scatterers [32].

2.1.3 Correlation Diffusion Equation (DCS)

In 1990s Boas et al. and Yodh et al. derived the correlation diffusion equation from correlation transport theory. The correlation diffusion equation describes the propagation of unnormalized electric field temporal autocorrelation function for turbid media. It provides a natural framework for tomographic reconstruction of tissue dynamics. Equation 2.9 represents the photon diffusion equation, which describes the photon propagation in tissue. In highly scattering media the tissue fluence rate, Φ (r,t) obeys time-dependent diffusion equation [32].

$$\nabla.(D\nabla\ \Phi(r,t))-v\mu_a\,\Phi(r,t) + vS(r,t) = \frac{\delta\Phi(r,t)}{\delta t} \qquad 2.9$$

where r is the position vector, v is the velocity of light in the medium, μ_a is the absorption coefficient, $D \approx v/3\mu_s'$ is the photon diffusion coefficient, where μ_s' is the reduced scattering coefficient in the medium. S(r,t) is the isotropic source term.

Under the same approximations the unnormalized temporal field autocorrelation (Equation 1.1) obeys a similar diffusion equation [32]:

$$\left[-\frac{1}{3\mu_s'}\nabla^2 + \mu_a + \frac{1}{3}\alpha\mu_s' k_0^2\langle\Delta r^2(\tau)\rangle\right] G_1(\vec{r},\tau) = S(\vec{r}) \qquad 2.10$$

Here, since the source is a continuous wave (CW), and the scatterer movement ($\langle\triangle\ r^2(\tau)\rangle$) acts as an effective "absorption" term for the attenuation of unnormalized electric field autocorrelation function [1]. Equation 2.10 could be solved using Laplace transform with the boundary conditions of semi-infinite geometry (See figure 7)

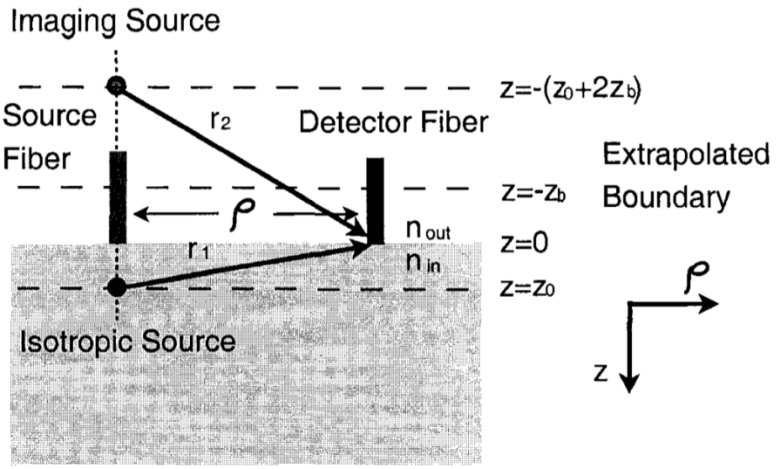

Figure 7: Illustration of Semi-infinite geometry

Here ρ is the distance between the source and detector fiber, $R_{eff} = -1.44n^{-2} + 0.71n^{-1} + 0.064n$, is the effective reflectance coefficient. Using these boundary conditions, we get

$$G_1(\rho,\tau) = \frac{3\mu_s'}{4\pi}\left(\frac{e^{-k_D r_1}}{r_1} - \frac{e^{-k_D r_2}}{r_2}\right) \qquad 2.11$$

Although the motion of RBCs may be considered as a random motion, David boas et al. found that the Brownian motion model showed better fitting in biological tissue. Therefore the measurement of $G_1(r,)$ can be used fitted to get the blood flow index ($BFI = \alpha D_B$). BFI is used to parameterize blood flow [3]. The relative blood flow, $rBF = \frac{BFI}{BFI_0}$, which is a deviation of BFI with respect to baseline is used to indicate the relative changes in blood flow for DCS.

2.2 DCS Technology

2.2.1 DCS instrumentation

The DCS system is designed similar to Dong et al 2012 paper [3]. It consists of a long coherence length (>10m) CW laser at 785nm (DL785- 100-S, ~100 mW, CrystaLaser, Reno, Nevada, USA) as the source. The detector used is a photon counting avalanche photo diode (APD) (SPCM AQRH-14-FC, Excelitas Technologies, Vaudreuil (Quebec), Canada). The output of the APD is transistor-transistor logic (TTL) pulses. The output of the APD is connected to a computer (CPU: Intel Core 2 Duo, RAM: 4 GB) with a 32-bit, 8 channel data acquisition card (PCI-6602, National Instruments) through a shielded BNC connector block (BNC-2121, National Instruments). The Light from the source is incident on the tissue sample using a multi-mode optical fiber of 125 μm diameter (M31L02, THORLABS). The light photons are collected using a single-mode optical fiber operating in few-mode configuration (P1-980AR-2, THORLABS). A single mode fiber (P1-780AR-2, THORLABS) was also used in early development of the system. The another end of the detector fiber is connected to the APD.

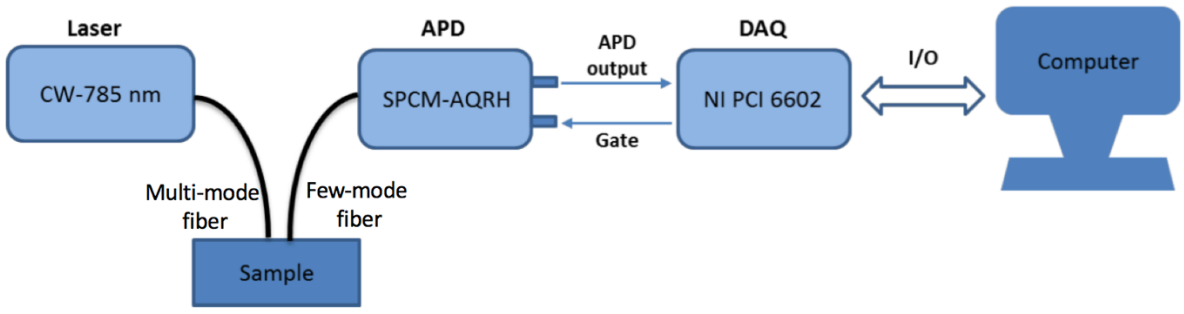

(a)

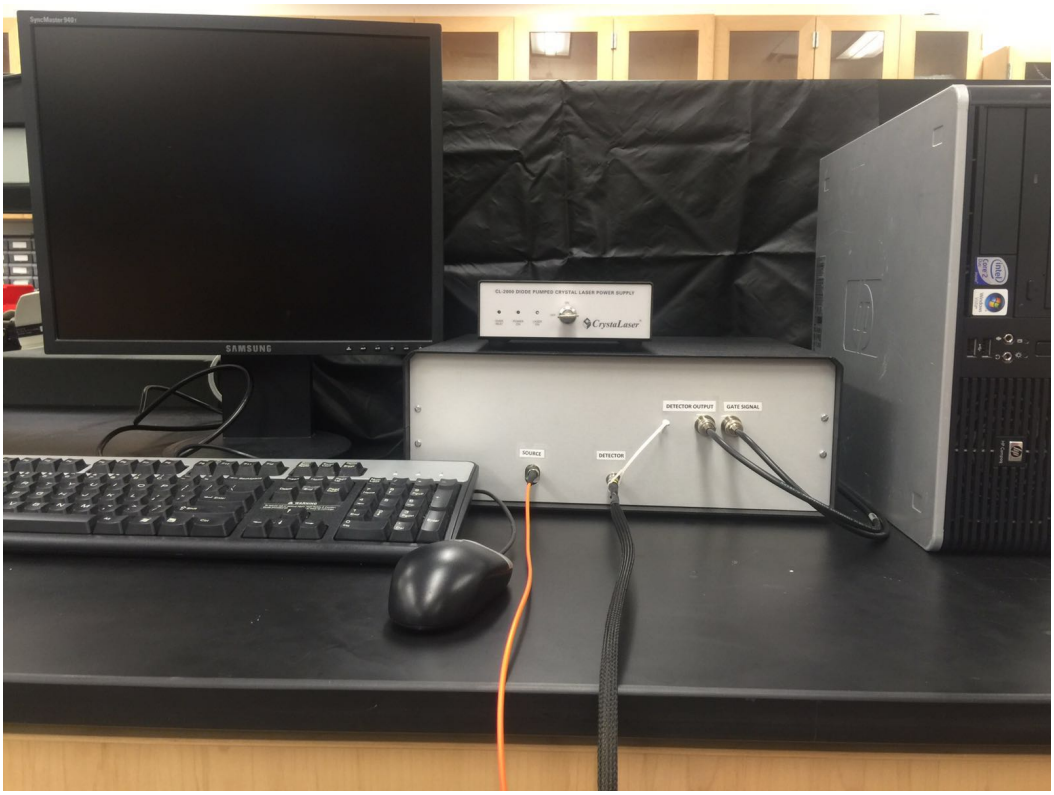

(b)

Figure 8: (a) Block diagram of DCS system. (b) A photograph of DCS system

2.2.2 Fiber-Optic Probe

DCS enables use of large variety of probes. The most basic probe consists of source-fibers (multimode) and one or more detector fibers (single or few-mode). For an optical fiber the number of guided modes is dependent on the core radius (a), relative-refractive index (N_A), also known as numerical aperture and the operating wavelength (λ). The relation between the number of modes and the properties of a dielectric optical waveguide is described by introducing a normalized frequency V [40].

$$V = \frac{2\pi a}{\lambda} N_A \qquad 2.12$$

When V is smaller then the critical cutoff frequency V_C only fundamental mode LP_{01} can be guided through the fiber. When V is greater than V_C the fiber can guide more than one mode and becomes a few-mode fiber [40]. The number of optically guided modes allowed by a single-mode fiber is given by $V^2/2$. We are using a few-mode fiber (P1-980AR-2, THORLABS) which can pass 5 guided modes in the detector fiber. The separation between the source and detector is 1.5 cm. Improving the SNR of is crucial when the detected signal is extremely low, which is not unusual for DCS systems, especially with larger source-detector separations. Using few-mode fiber the light intensity detector is significantly increased, thus improving the SNR of the DCS system [40].

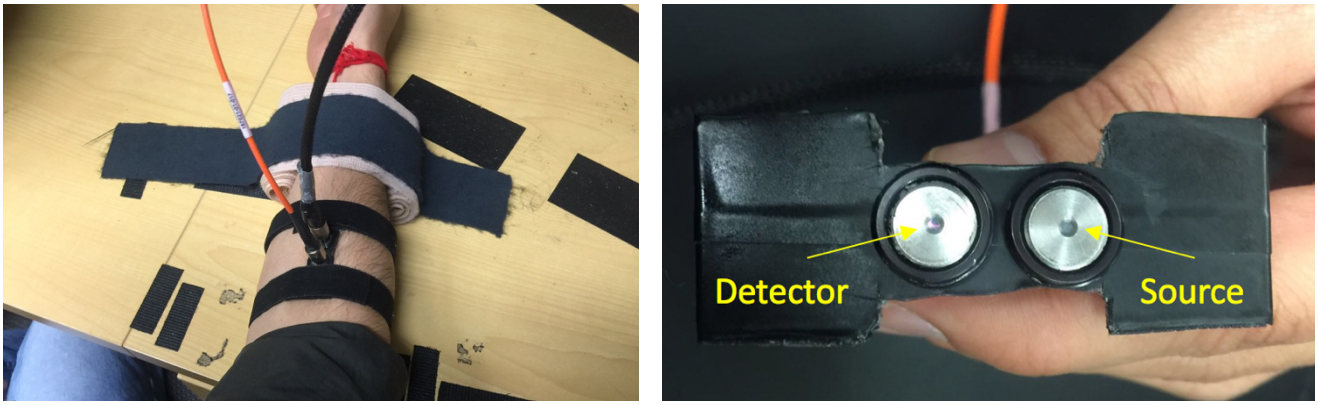

(a) (b)

Figure 9: (a) : DCS probe setup on arm. (b) DCS fiber optic probe

2.3 Data Acquisition and Processing

2.3.1 Data Acquisition Principle

Data acquisition was done using National Instruments' LabVIEW software. Two virtual instruments (VI) were designed for DCS system in LabVIEW. The first VI generates a gate signal to drive the APD and the second VI is responsible for signal acquisition and recording. The TTL output from the APD were counted over sampling time τ by counter/timer board. The PCI-6602 has maximum frequency of 80MHz, which means the fastest input pulses that can be counted are 12.5ns (1/80,00,000 s) apart [3]. The PCI-6602 is a 32-bit counter and can count upto 4,294,967,295 ($2^{32} - 1$) before it rolls over. The buffer size was limited and overflowed in less than 1 second for time resolution of anything less than 2μs [3]. The sampling rate of the system can reach upto ~400kHz and thus enables minimum lag time of ~2.5 μs, which is significantly shorter than the decay constant in DCS applications [3]. For stable data acquisition experiments were conducted at 4.0 μs [36].

A gate signal was used to count the APD output pulses. The gate signal has a total time resolution of 4 μs with 80% duty cycle. Buffered period measurement technique was used for counting photon pulses [36]. In buffered period measurement, source edges cause to increment while gate edges will buffer the instantaneous count and also reset the count register back to 0 for the next interval (see figure 10). Thus for our application every APD pulse will increment the internal count register and every active gate edge will store the instantaneous count value in the task buffer and reset the count register to 0. The period of gate signal is characterized in terms of APD pulses that occur per interval. To accomplish this, the DAQmx Timing VI was set up to use "implicit" timing (see figure 11 (d)) [36]. This

means the signal whose period is being measured sets the timing of sampling based on whenever its edges arrive [34]. Thus the net effect is to perform "binning" measurement where the "periods" is read to find out how many APD pulses where recorded within each interval of the gat signal. When using buffered counter operations, the first acquired points represented bad data in period measurements and thus were ignored. The first data point is the measured interval between the instant when the counter is armed and when the first edge transition takes place on the counter GATE (refer figure 10) [35]. Since there is no deterministic way of specifying when the counter is actually armed, the first value may be incorrect. Subsequent data points acquired will not have this problem and thus the first reading is ignored [35].

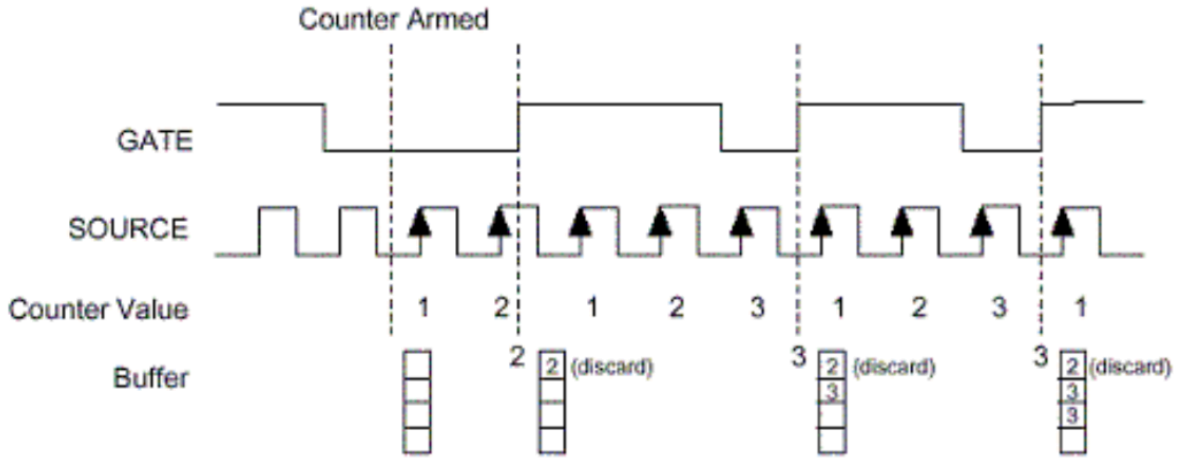

Figure 10: Buffered Period Measurement

We applied "queue" structure to link the "producer" and "consumer" loop in the second VI (see figure 11(d)). The "producer" loop was responsible for reading photon counts and the "consumer" loop was in charge of writing the data in a file. The two loops work in parallel for faster speed [3]. The data was read and stored for every 1 second with a 1 or 4

second delay between consecutive reads depending on the type of measurement. The data is stored in a binary format ".tdms" which is more efficient for storage of large data sizes. The following are the snippets of the Vis from LabVIEW.

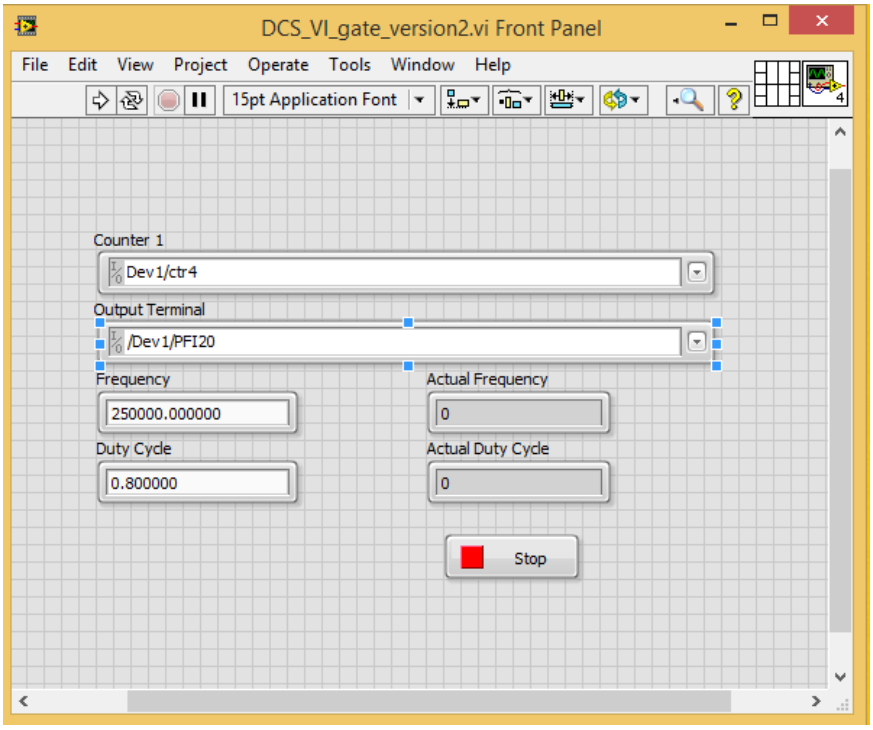

Figure 11 (a): Front panel of gate signal VI

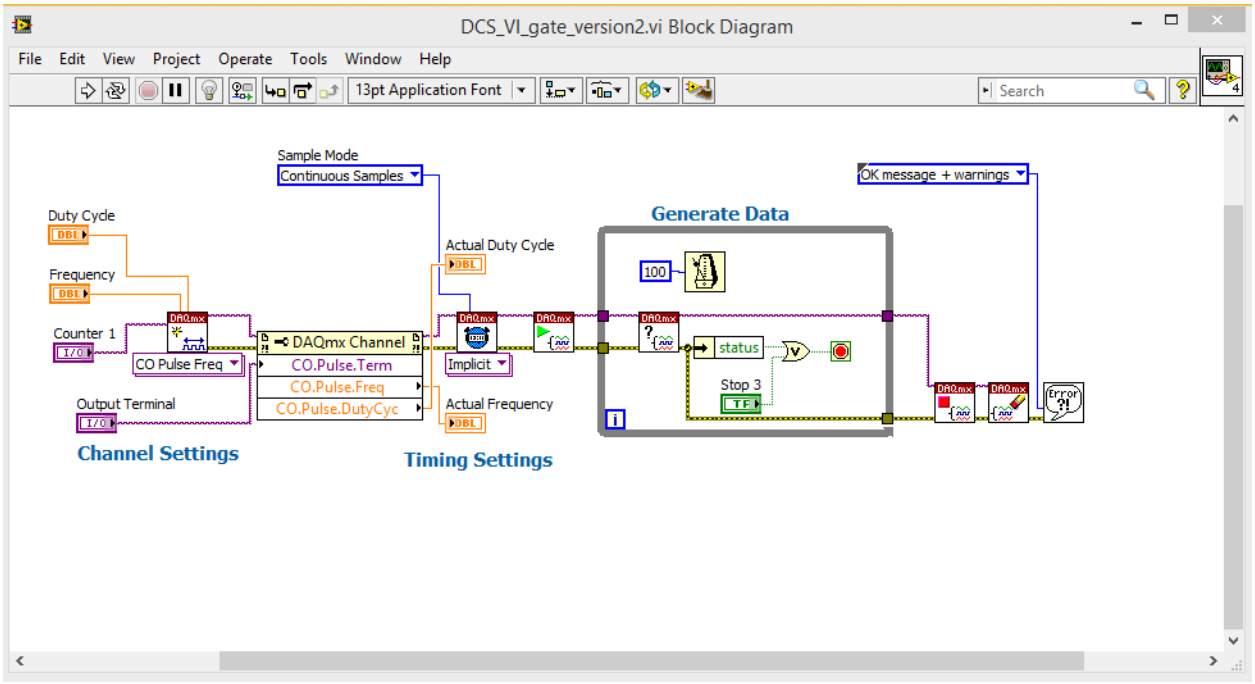

Figure 11 (b): Block diagram of gate signal VI

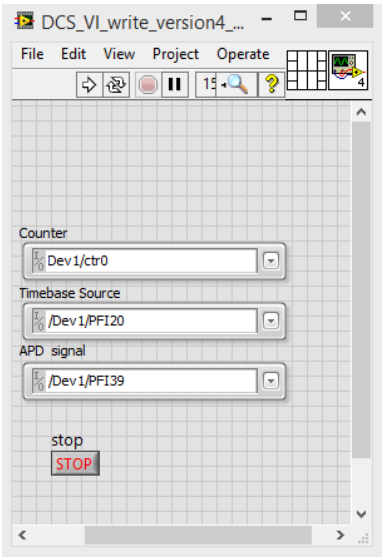

Figure 11 (c): Front Panel of read and write VI

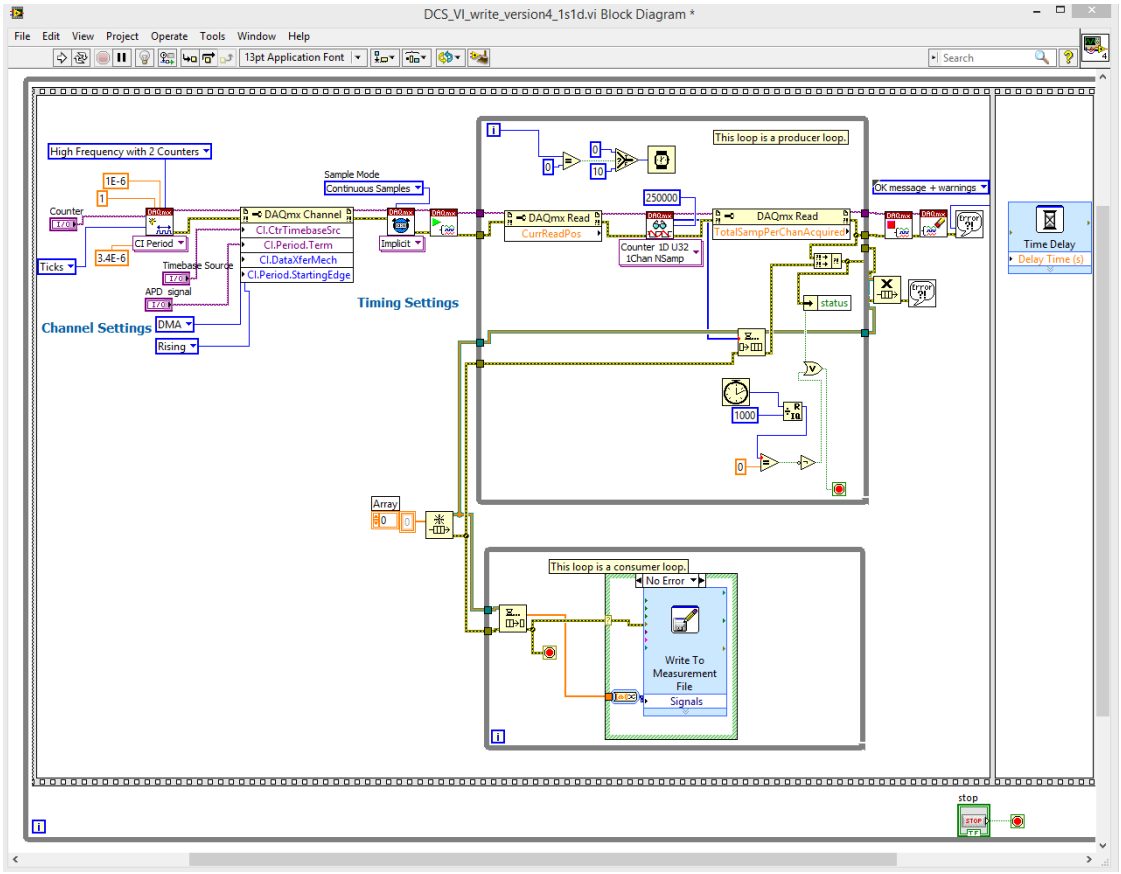

Figure 11 (d): Block diagram of read write VI

The acquisition system was tested its efficiency for counting photons. Two tests were performed: (1) First test was done to check the frequency and duty cycle of the gate signal. It was found that the system is most efficient at 80% duty cycle. (2) The second test was done to determine the photon counting efficiency of the read and write VI by varying frequency of the APD signal. The VI showed a good efficiency of ~93% till 20MHz and 30MHz frequency for sine and square as APD signal respectively [36].

2.3.2 Data Processing Principle.

The data from LabVIEW is loaded into MATLAB. The output file has the photon counts for each active gate signal. MATLAB was used to calculate the rBF using curve-fitting of the correlation diffusion equation. Autocorrelation was calculated using MATLAB's native "autocorr" function. The "autocorr" function computes the sample autocorrelation function of a univariate, stochastic time series [39]. The autocorrelation gives is unnormalized intensity autocorrelation (G_2). By normalizing G_2 we get g_2 which is the normalized intensity autocorrelation function. The normalized g2 obtained experimentally is fitted in the correlation diffusion equation to obtain Db. Db is directly related to the BFI with respect to baseline.

2.4 Validation of DCS System

For validation of DCS system we performed 2 experiments (1) using intralipid phantom and (2) In Vivo arm-cuff occlusion experiment.

2.4.1 Intralipid phantom experiment

Intralipid phantoms play an important role in the development of diagnostic systems [40]. It can be used for purposes of initial testing of system design, optimizing the signal to noise ratio (SNR) of the existing system [41]. In order to validate and assess the ability of the system, an intralipid phantom was prepared as shown in figure 12

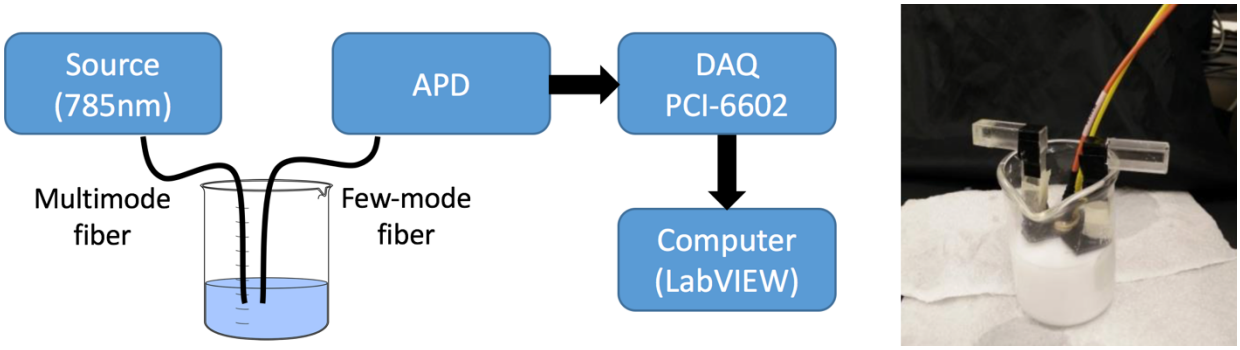

(a) (b)

Figure 12: (a) Schematics of DCS experiment setup. (b) intralipid phantom.

Intralipid phantom of Different concentrations were prepared to mimic the characteristics of the tissue. The intralipid concentrations used were 0.3%, 0.5%, 0.7% and 1%. The validation test was also done on a solid phantom with $\mu_a = 0cm^{-1}$ and $\mu_s' = 5cm^{-1}$[36]. The Schematic of the setup is shown in Figure 12(a)**.** The separation between source and detector fibers was 1 cm.

The data acquired was processed in MATLAB. The normalized intensity autocorrelation was obtained for all the test samples. The results obtained showed a similar trend to results of previous studies (see figure 13).

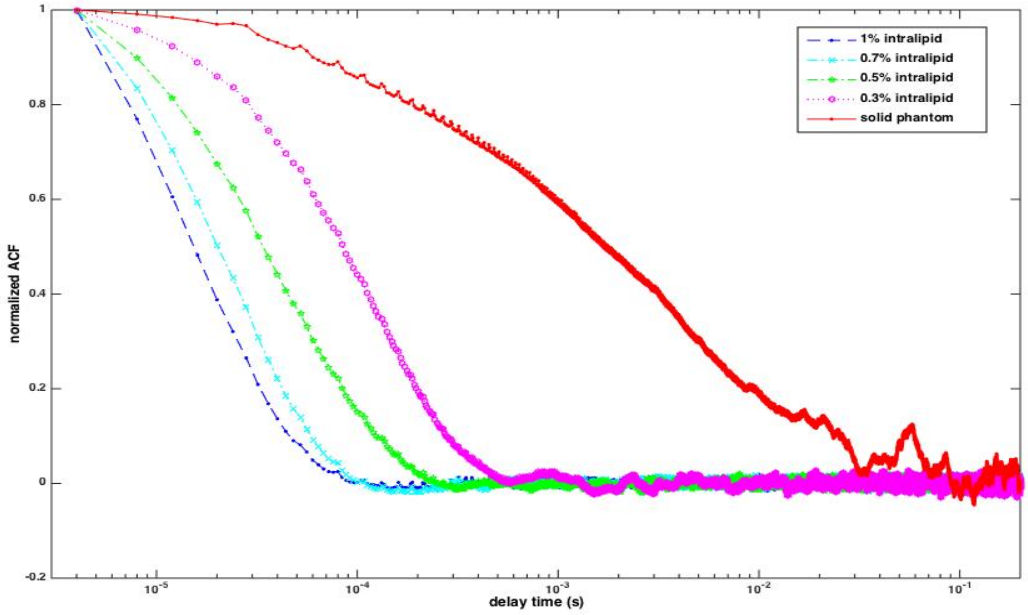

Figure 13: Normalized intensity autocorrelation plots

2.4.2 In Vivo Arm-cuff Occlusion Experiment

The in vivo arm-cuff occlusion experiment was performed on healthy adults of either sex, of age group ranging from 23-40 years from by race and ethnic background. In order to vary the blood flow speed, a cuff on the subject's upper left arm was constricted for 30 seconds for a temporary vascular occlusion. The source-detector separation was 1.5cm and the probes were located on the forearm. The cuff inflation pressure was 200mmHg.

The data was recorded for 1 second with a delay of 4 seconds. The stored data was then processed using the script developed in MATLAB. Figure 14 shows the normalized autocorrelation functions of cuff occlusion stages, viz – baseline, occlusion, just after removal of occlusion and recovery of a single subject. Figure 15 shows the representative time response of relative blood flow (rBF) during occlusion experiment.

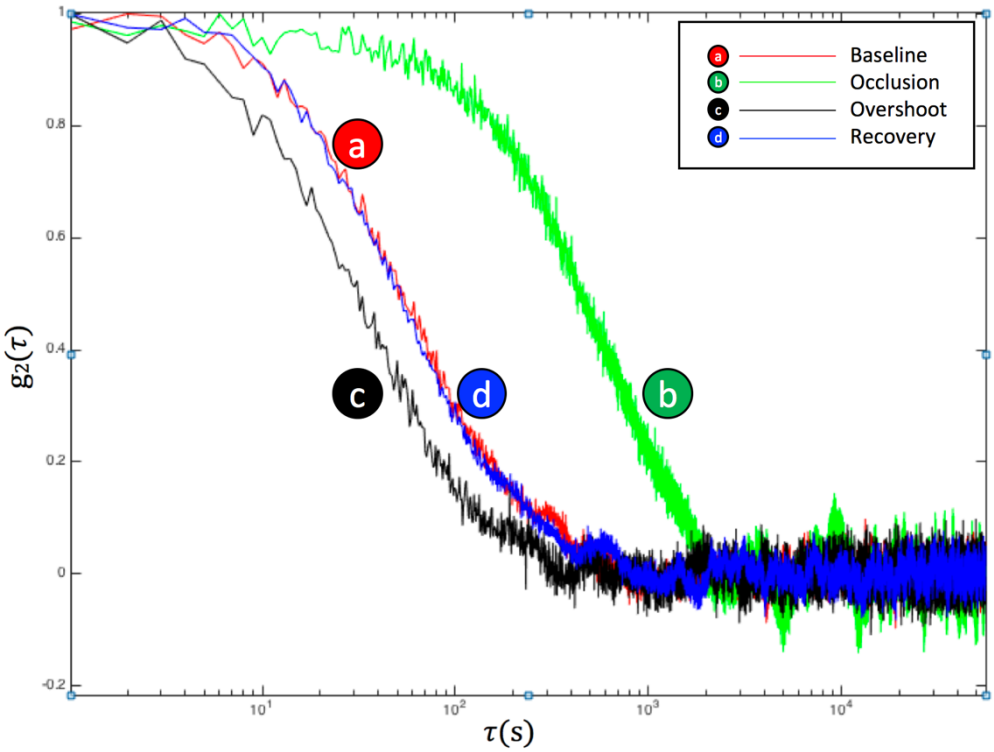

Figure 14: Autocorrelation function of cuff occlusion experiment

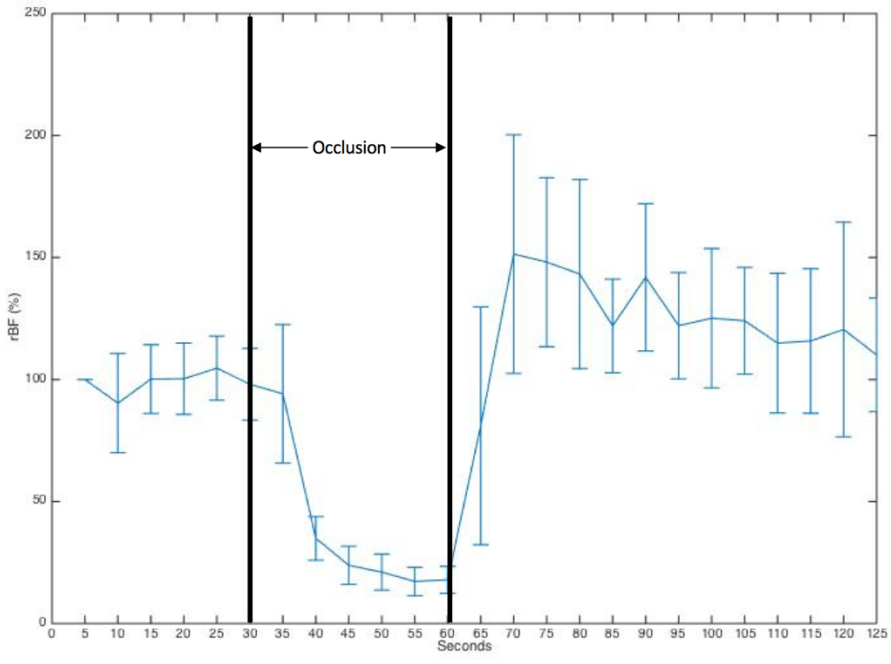

Figure 15: Errorbar plot for rBF plot of 8 subjects during arm-cuff experiment

The decay rate of g_2 shows significant change in figuer14. From figure 15 we can see that the blood flow was relatively constant for the baseline period of 30 seconds as no constriction was applied. Once the arm was occluded, the blood flow decreased with a sharp drop and when the constriction was released the blood flow immediately showed an overshoot followed by a slow decrease to the baseline due to homeostasis [3].

Chapter 3

Physiological Effects of LLLT

The aim in this part of the study is to explore how a single treatment of LLLT alters the blood perfusion in biological tissue. We performed LLLT treatment on the forearm of the subjects and recorded the changes in blood perfusion using DCS system described in the previous chapter.

3.1 Subjects and Ethical approval

Healthy young individuals of either sex, of age group ranging from 23-40 years from any ethnic background were considered. Interested participants were scheduled immediately for the experiment. On the day of each experiment the participants were given an oral explanation and then the participant was given the opportunity to ask questions. After their approval to start the experiment the participants' gender and age was recorded and the experiment was carried out. The participants were asked to keep the body stable as movement could produce motion artifacts. The participant was given the choice to stop the experiment if he/she felt uncomfortable.

3.2 Instrumentation

The LLLT treatment was administered with a 1064nm laser (CG-5000, HD Laser Centre, Dallas, TX, USA). This laser is FDA approved and is safe for various uses on humans, such as for improving circulation, temporary relief of muscle and joint pain, muscle spasm, stiffness associated with arthritis and relaxation of muscle tissue [41]. All the personnel who operated the CG-5000 laser in this study had been trained and certified by Dr. Rudy Rivera the Laser Safety Officer and Director of Research, Education and Operations from Cell Gen Therapeutics.

The laser was operated at 3.5 Watts and the diameter of the CG-5000 laser is 4cm. The power density used was ~280mW/cm^2 which is the same used in previous studies [41]. At this

power level, the energy emitted by the laser is very low, heat produced is very less and it is not harmful to human tissue [43].

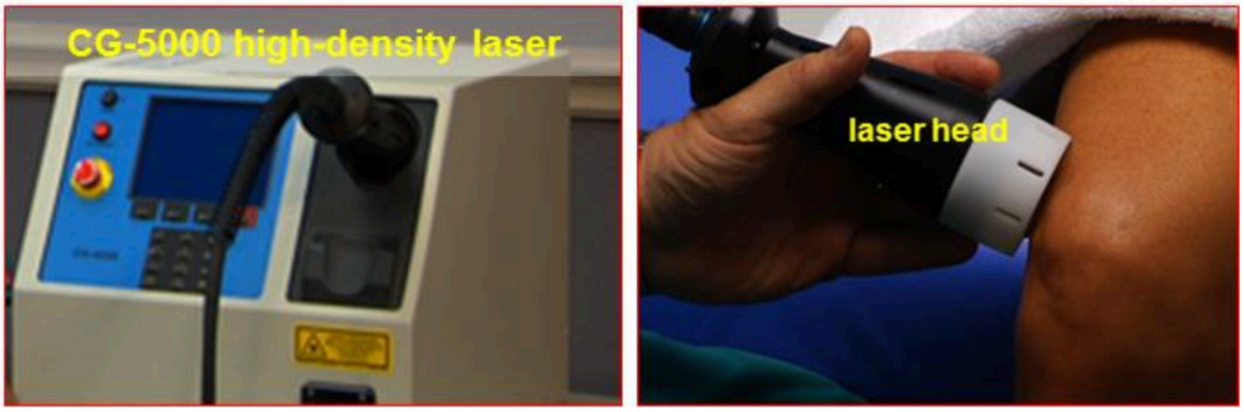

Figure16: (a) The CG-5000 laser used for LLLT. (b) The laser head which delivers the light to skin.

The DCS is used for acquisition of blood perfusion data during the LLLT experiment. The data is acquired and stored for every 1 second with a 1 second delay between consecutive reads. Figure 17 shows the setup of the LLLT experiment.

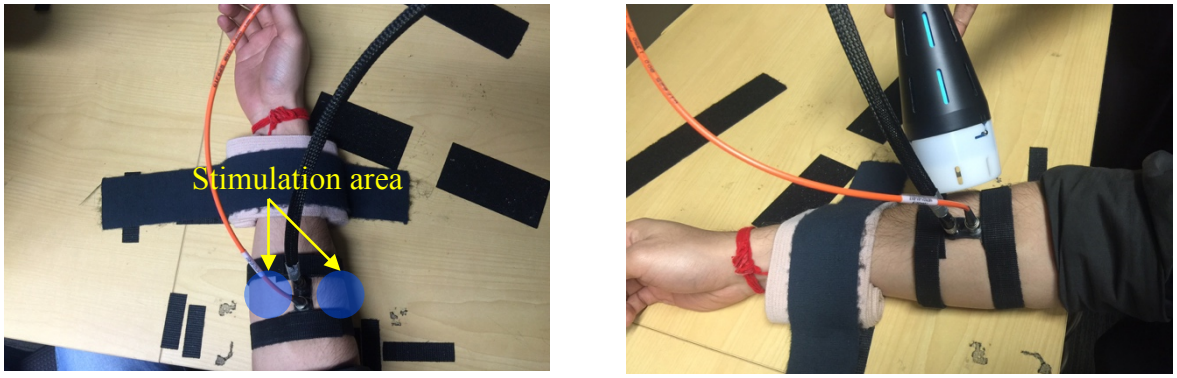

(a) (b)

Figure 17: (a) DCS probe setup. (b) DCS setup with LLLT stimulation.

3.3 Protocol

In each experiment, the DCS probe was placed on the subject's forearm as shown in the figure 17. The probe has two optical fibers, one acts as a source of the DCS system and one detector fiber. The source detector separation was 1.5cm. Once the probe was in place the subject was advised not to move as it may cause motion artifacts. The probe was secured in place using Velcro straps. The baseline readings were taken for first 2 minutes of the experiment. Then the forearm was stimulated using LLLT in 8 cycles of "on" and "off". The laser was on for 1 minute and off for 20 seconds. While the LLLT laser was on, the APD and the DCS source laser was turned off to avoid damaging the APD and avoid the accumulation of power due to source laser. The source laser and the APD were turned on during the treatment when the LLLT was off to record the data. The treatment was for 8 minutes. Each one-minute treatment cycle was marked by a timer counting down and by a alarm from the apparatus. After the LLLT stimulation, the subjects were asked to sit for another 7 minutes during which DCS data was recorded. The aim of this recovery is to see where the change in the rBF due to treatment was maintained or reversed after the LLLT. The total time for the experiment was ~20 minutes (see figure 17).

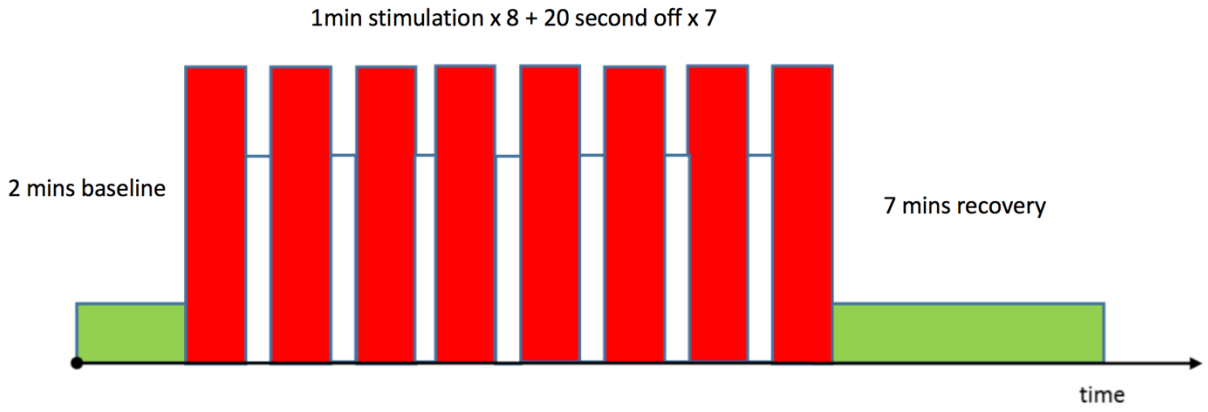

Figure 18: LLLT Stimulation Protocol

The experiment was conducted in a locked room with black walls and no reflective surfaces. The experimenters locked both themselves and the participants inside the room, which has a sign on the outer door indicating that the apparatus was in use, and made sure that 1064nm protective eyewear was worn by all individuals present in the room, though the precaution was also taken that while LLLT stimulation was done, light was not shined in the eyes.

3.4 Data Processing and Analysis Methodology

The data was acquired from DCS system and processed in MATLAB. Data was processed for individual subjects and visually inspected to exclude data points associated with significant data discontinuities or high noise. An average of 3 data points during the treatment were taken and averaged. Similar was done at every acquisition point and average was taken to remove high frequency noise. Thus after averaging, a total of 17 data points were picked from the baseline, during the 10 minute treatments and from the 7 minutes of recovery. The first minute of data was rejected as it showed inconsistency. This process was done for each subjects. Figure 19 shows the processed data from one subject.

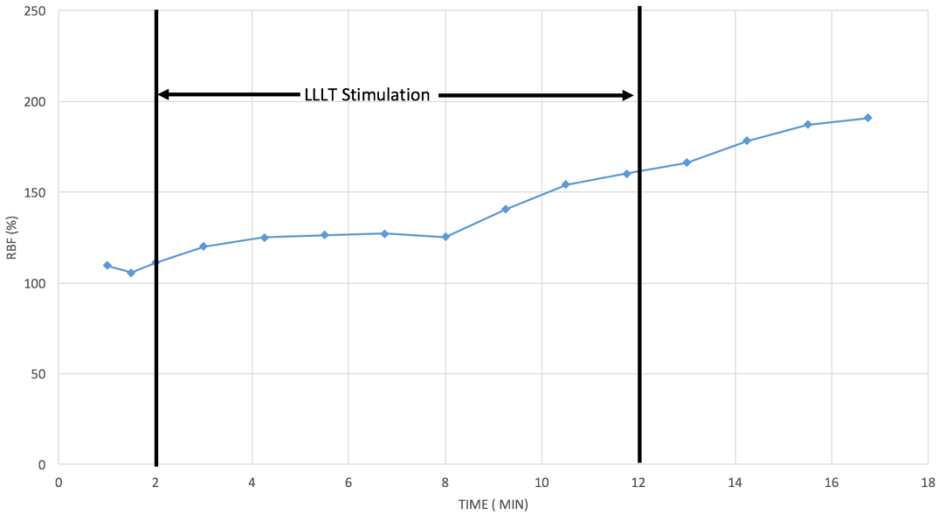

Figure 19: rBF plot for LLLT stimulation experiment

3.5 Statistical Analysis

Statistical analysis was performed to examine whether the treatment-induced change in blood perfusion was statically significant. ANOVA was performed to evaluate if any of the 17 data points were statically significant at a confidence interval of 95%. The null hypothesis stated that there was no significant difference pre and post treatment in rBF. The alternative hypothesis states that there was significant difference between data obtained during baseline and after treatment. The test was done for the average of the grouped data. Figure 20 shows the distribution of data.

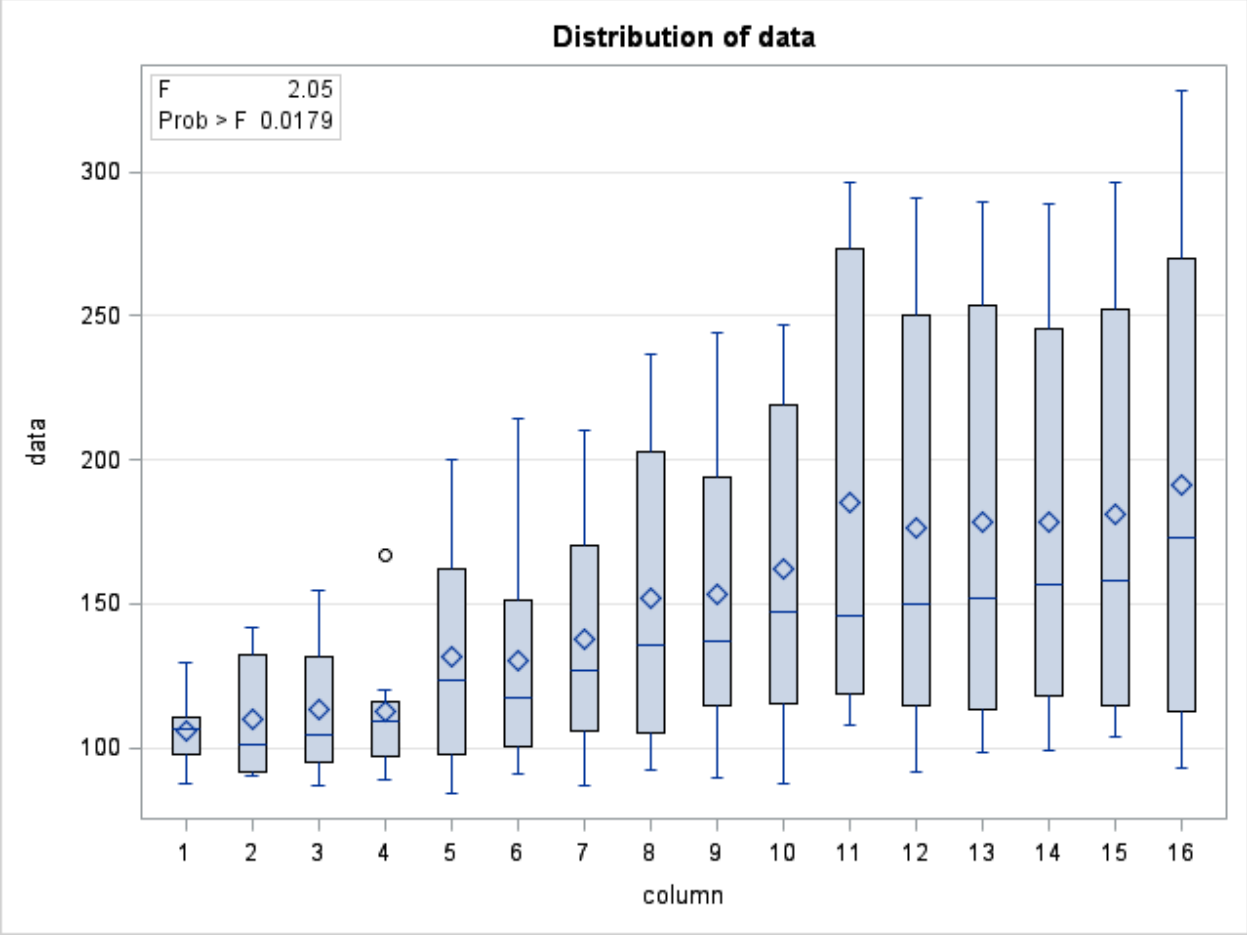

Figure 20: Distribution of data obtained using ANOVA

3.6 Results

The study had 8 subjects who participated for the experiment. The subject demographics are shown below:

Table 2: Subject Demographics

Subject No.	Gender	Age
Subject 1	Female	23
Subject 2	Female	24
Subject 3	Male	40
Subject 4	Male	23
Subject 5	Male	26
Subject 6	Male	23
Subject 7	Male	25
Subject 8	Female	24

The results of changes in rBF obtained are shown in figure 20. The results show that there is clear increase in the rBF after LLLT treatment. The statistical analysis confirmed the changes in rBF to be significant. The results shows there is significant difference between the baseline rBF and the rBF during recovery period after LLLT stimulation. This signifies that the LLLT results in increased blood perfusion which means more blood is supplied to the tissue post LLLT treatment.

Chapter 4

Discussion and Future Work

4.1 Discussion

4.1.1. Diffused Correlation Spectroscopy

In recent years, DCS has been employed as a viable technique to monitor deep tissue blood perfusion (rBF). DCS blood perfusion measurement is accomplished by monitoring speckle fluctuation of photos due to the moving scatters in the biological tissue. RBCs are the main source of this scattering inside blood vessels. DCS provides some unique features such as measurement of blood perfusion in tissue microvasculature, non-invasiveness, high temporal resolution (upto several milliseconds), portability and high penetration depth (upto several centimeters). DCS Technology has been extensively validated in various tissues through comparisons with laser Doppler flowmetry, power Doppler ultrasound, Xenon-CT, florescent microsphere flow measurement and arterial spin labeled magnetic resonance imaging (ASL-MRI) [40].

In this study we have demonstrated an implementation of DCS system with a software based autocorrelator based on National Instruments' LabVIEW and MATLAB. The software correlator has been validated by an intralipid phantom and in vivo arm-cuff occlusion experiment. It is easy to operate and relatively cost-effective. Although the data sampling speed is moderate, the minimum lag time is much shorter that the decay constant of g_2. Thus, the extraction of the required parameter is valid. Also smoother starting and ending plateaus improve the accuracy of the curve fitting and thus, in the BFI. The system holds potential of being a real-time, bead side monitoring device and can be used in research and clinical setting.

4.1.2 Physiological effects of LLLT

In recent years, LLLT has been used in the areas of physical medicine and rehabilitation. Its applications startedmainly for wound healing and pain relief, but over the recent years they have broadened to include diseases such as stroke, myocardial infraction and degenerative traumatic brain disorders [41,42]. The aim of this study is to evaluate the effects of a single session of LLLT on tissue blood perfusion.

Due to the effect of LLLT on mitochondria, nitric oxide (NO) is photodissociated from the cytochrome c oxidase. NO is a free radical gas and an endogenous vasodilator [14]. Studies by R. F. Furchgott demonstrated the ability of light to influence localized production and release of NO and cause vasodilation thus increasing blood flow. The wavelength which mediated NO are different from LLLT being in the blue and ultraviolet range. Many studies described the increase in animal blood flow during and after LLLT. This could be the result of the production of CO_2 in the TCA cycle. CO_2 dilates the blood vessels and increases the blood flow due to hypercapnia [27].

4.2 Limitations

4.2.1 Limitations of DCS

Current DCS technology calculates BFI based on semi-infinite geometry where the tissue is considered homogenous. As a result, the BFI indicates a BFI not only for skeletal muscle, but also fat and also skin as light penetrates all these tissues as well [44]. The throughput of single-mode and few-mode fibers is relatively low especially when the source detector separation is >2cm. This causes a drop in SNR ratio. This SNR becomes more of an issue with the presence of hair and dark skin. To overcome this issue many groups have used a bundle of fibers with multiple detectors. However, this approach is very expensive that it requires many APDs. Another method

to improve SNR is by delivering more power to the tissue through source fiber; however, the ANSI standards for skin exposure must be considered and the light exposure should be kept within safe limits. Finally, a significant limitation of DCS is its vulnerability to motion effects. Securing the probe firmly as possible to the subject without obstructing the flow reduces these motion artifacts.

4.2.2 Limitations of LLLT study

In evaluation of the physiological effect of LLLT produced a significant hemodynamic change at a 95% confidence interval for sample size of 8 subjects. However, it is still unclear as to whether the increased BFI was due to Nitric Oxide or CO_2 or some third reason altogether. Another limitation was absence of a placebo-controlled/ sham group. Including this into the study would rule out the possibility of placebo effects and would give a more decisive result. Further study is needed to explain and interpret the underlying mechanism on this result. Another Limitation is the concern of temperature induced by the LLLT laser which may cause vasodilation due to homeostasis and increase blood flow. Thus the parameter should also be taken into account in further studies.

4.3 Future Work

4.3. Diffused Correlation Spectroscopy

DCS could be developed as a safe, inexpensive, and portable modality from clinical perspective. It could be used as a bedside monitoring in intensive care unit ad operating room. DCS could provide complimentary information to NIRS per microvascular BFI and regional oxygen delivery as a result. NIRS and DCS could be combined to obtained regional $CMRO_2$. DCS has the potential to help scientists develop diffused optical tools to increase our understanding of neurovascular coupling and early brain development [45]. The current DCS setup could be

developed to monitor real-time changed in blood perfusion. Another development of a dual wavelength DCS system which would give us insight in the levels of Hb and HbO along with BFI.

4.4. Low Level Laser Therapy

Since LLLT is non-invasive, future studies could test this treatment over a larger subject group without any additional concern. The question of possibility of the increase of low-frequency rhythms of regulation of blood microcirculation due to LLLT still remains open and demands additional research. This is because the system of microcirculation is very variable and very adaptable under and without external influences. Also additional research is required for the explanation of temperature threshold [46].

APPENDIX A

Thermal effect of LLLT

Thermal effect of LLLT

The future work of my thesis is the study of temperature induced by LLLT laser. This study would help us understand the effect of the temperature induced and its contribution towards the increase in rBF during LLLT treatment. I have been study the cause of the increased rBF during LLLT. This section discussed the setup and the comparison of LLLT with the thermal measurement.

A.1 Experimental Setup.

In order to compare the LLLT and thermal stimulation, the setup was kept the same. Medoc's PATHWAY Pain & Sensory Evaluation System (see figure A-1) was used to replicate the temperature induced due to LLLT laser. The DCS probe was attached on the arm in the same way as that of LLLT measurements and the thermal stimulation was induced on both the sides of the probe similar to the LLLT treatment. Same protocol was used to induce temperature. The temperature stimulation was 38^{o}C and 32^{o}C as the baseline (refer section 3.3 for protocol). The temperature was selected by measuring the temperature induced by the LLLT laser and recording it with a thermal probe (TSP01, THORLABS).

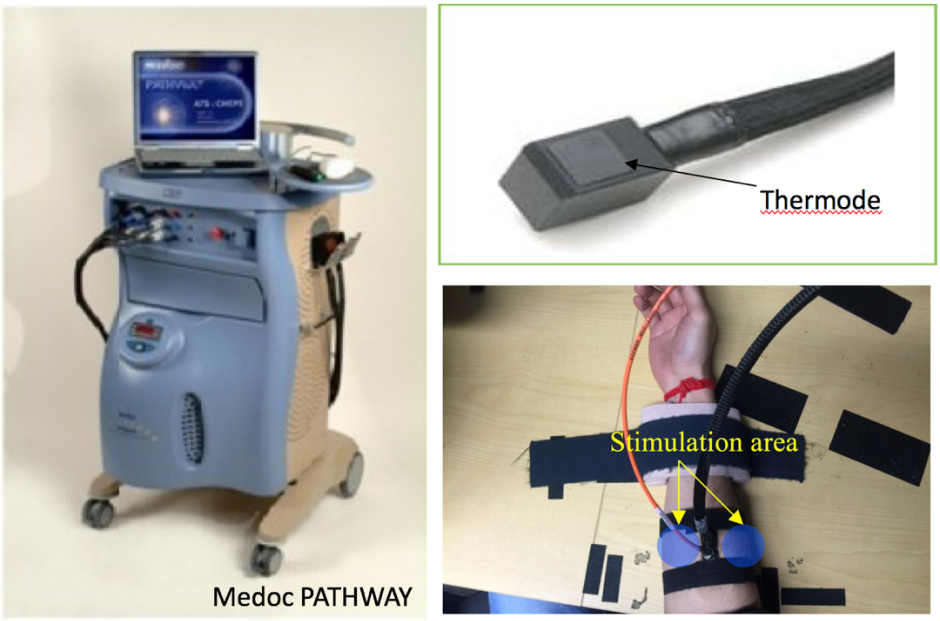

Figure A-1: DCS setup with thermal stimulation

A.2 Data Processing

The data acquired by the DCS system was processed using MATLAB. For individual subjects the data was visually inspected to exclude data points associated with significant data discontinuities or high noise. An average of the data was taken for each minute to remove hogh frequency motion artifact components. Thus after averaging 17 data points were acquired including baseline, thermal stimulation and recovery. The first minute data was rejected as it showed incontinency. This process was repeated each of the subjects. The same subjects were called for the thermal study for better comparison between the LLLT and Thermal stimulation. The average of the group data was taken and plotted along with the LLLT stimulation data against time to compare both the studies (see figure B-2).

A.3 Result

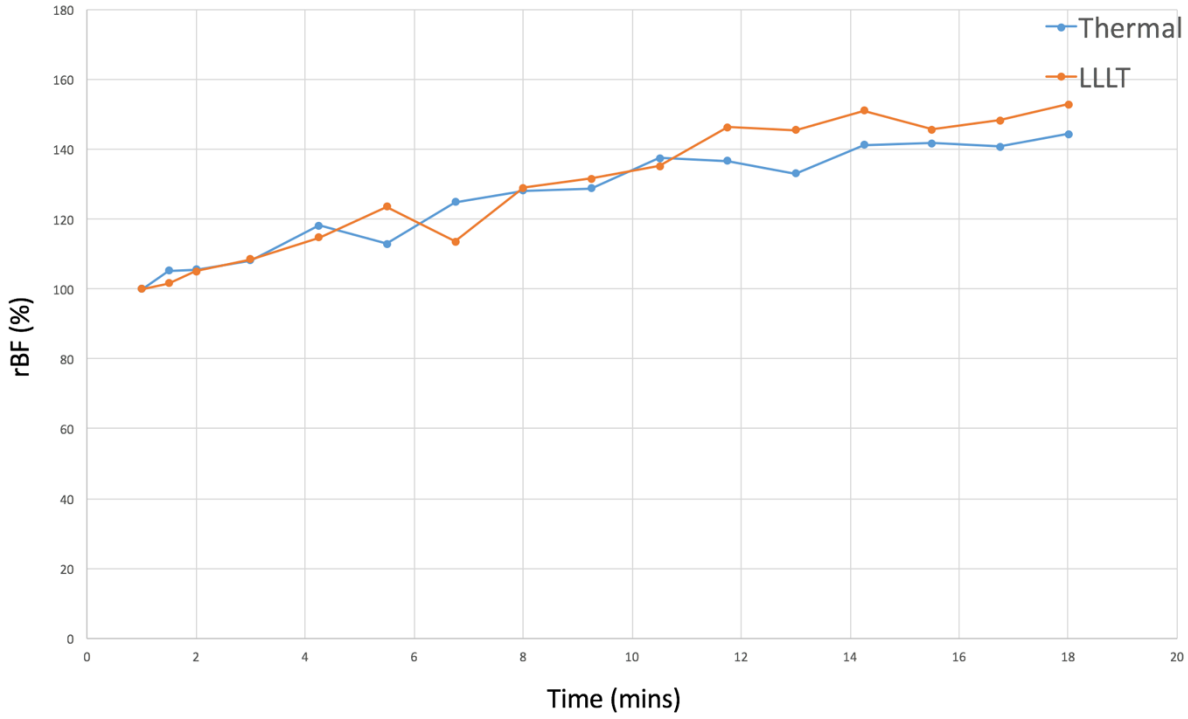

Figure A-2: Comparison between LLLT and Thermal Stimulation

From the result we can see that the response is very similar for LLLT and thermal stimulation in the case of grouped data. Thus we can conclude that blood perfusion increased due to the temperature induced by the LLLT stimulation. However, we also observed in the case of individual subjects that the response is always not the same. This may be due to the fact that each subject with different scattering and absorption properties of the tissue, absorbs different amount of light and produces different amount of heat in the tissue.

Thus we can conclude that the LLLT does induce some temperature in the tissue, resulting in increased blood perfusion due to homeostasis. Thus the increased blood perfusion due to LLLT is the sum of the heat induced and some other physiological effect induced due to the incident of NIR light on the tissue.

References

1. David B. (1996). *Diffuse photon probes of structural and dynamical properties of turbid media: theory and applications* (Unpublished doctoral dissertation). University of Pennsylvania, Philadelphia, U.S.A.
2. Jing D., Renzhe B. & Kijoon L. (2015). *Frontiers in Biophotonics for Translational Medicine.* Retrieved from http://books.google.com
3. Dong_J. *et al. Diffuse correlation spectroscopy spectroscopy with fast Fourier transform-based software autocorrelator*. J. Biomed. Opt. **17**,97004 (2012).
4. Wang, L.V. & Wu, H. in *Biomedical optics: principles of imaging* (Wiley-Interscience, Hoboken, N.J, 2007).
5. Jobsis, F. (1977). *Noninvasive, infrared monitoring of cerebral and myocardial oxygen sufficiency and circulatory parameters*. Science, 198(4323), 1264-1267. doi:10.1126/science.929199
6. Phan, T. G. & Bullen A. Practical intravital two-photon microscopy for immunological research: faster, brighter, deeper. *Immunol Cell Biol.* **88**, 438-444 (2010).
7. Bunce, S. C., Izzetoglu, M., Izzetoglu, K., Onaral, B. & Pourrezaei, K. Functional near- infrared spectroscopy. *Engineering in Medicine and Biology Magazine, IEEE* **25**, 54-62 (2006).
8. Chance, B., Cope, M., Gratton, E., Ramanujam, N. & Tromberg, B. Phase measurement of light absorption and scatter in human tissue. *Rev. Sci. Instrum.* **79**, 3457-3481 (1998).
9. Villringer, A. & Chance, B. Non-invasive optical spectroscopy and imaging of human brain function. *Trends Neurosci.* **20**, 435-442 (1997).

10. Cheung, C., Culver, J. P., Takahashi, K., Greenberg, J. H. & Yodh, A. G. In vivo cerebrovascular measurement combining diffuse near-infrared absorption and correlation spectroscopies. *Phys. Med. Biol.* **46**, 2053 (2001).

11. JC, R. & F, G. Low-level light therapy of the eye and brain. *Eye and Brain* **2011**, 49-67 (2011).

12. Miller, E. K., Freedman, D. J. & Wallis, J. D. The prefrontal cortex: categories, concepts and cognition. *Philosophical Transactions of the Royal Society B: Biological Sciences* **357**, 1123-1136 (2002).

13. Hatefi, Y. The Mitochondrial Electron Transport and Oxidative Phosphorylation System. *Annu. Rev. Biochem.* **54**, 1015-1069 (1985).

14. Hamblin, M. R. (2008). The role of nitric oxide in low level light therapy. Mechanisms for Low-Light Therapy III. doi:10.1117/12.764918

15. Karu, T. Primary and secondary mechanisms of action of visible to near-IR radiation on cells. *Journal of Photochemistry & Photobiology, B: Biology* **49**, 1-17 (1999).

16. Santana-Blank, L., Rodriguez-Santana, E. & Santana-Rodriguez, K. Theoretic, Experimental, Clinical Bases of the Water Oscillator Hypothesis in Near-Infrared Photobiomodulation. *Photomedicine and laser surgery* **28**, S41-S52 (2010).

17. Huang, Y., Sharma, S. K., Carroll, J. & Hamblin, M. R. Biphasic Dose Response in Low Level Light Therapy: An Update. *Dose-Response* **9**, 602-618 (2011).

18. Karu, T. Mitochondrial Mechanisms of Photobiomodulation in Context of New Data about Multiple Roles of ATP. *Photomedicine and Laser Surgery* **28**, 159-160 (2010).

19. .J. Ehrreich and R.F. Furchgott, Relaxation of mammalian smooth muscles by visible and ultraviolet radiation, Nature 218 (1968) 682-4.

20. R. Mittermayr, A. Osipov, C. Piskernik, S. Haindl, P. Dungel, C. Weber, Y.A. Vladimirov, H.

Redl and A.V. Kozlov, Blue laser light increases perfusion of a skin flap via release of nitric oxide from hemoglobin, Mol Med 13 (2007) 22-9.

21. L. Vladimirov, A., G.I. Klebanov, G.G. Borisenko and A.N. Osipov, Molecular and cellular mechanisms of the low intensity laser radiation effect, Biofizika 49 (2004) 339-50.
22. Y.A. Vladimirov, A.N. Osipov and G.I. Klebanov, Photobiological principles of therapeutic applications of laser radiation, Biochemistry (Mosc) 69 (2004) 81-90.
23. G.G. Borisenko, A.N. Osipov, K.D. Kazarinov and A. Vladimirov Yu, Photochemical reactions of nitrosyl hemoglobin during exposure to low-power laser irradiation, Biochemistry (Mosc) 62 (1997) 661-6.
24. T.I. Karu, L.V. Pyatibrat and N.I. Afanasyeva, Cellular effects of low power laser therapy can be mediated by nitric oxide, Lasers Surg Med 36 (2005) 307-14.
25. G.A. Guzzardella, M. Fini, P. Torricelli, G. Giavaresi and R. Giardino, Laser stimulation on bone defect healing: an in vitro study, Lasers Med Sci 17 (2002) 216-20.
26. H. Tuby, L. Maltz and U. Oron, Modulations of VEGF and iNOS in the rat heart by low level laser therapy are associated with cardioprotection and enhanced angiogenesis, Lasers Surg Med 38 (2006) 682-8.
27. Hamblin, M. R. (2008). The role of nitric oxide in low level light therapy. Mechanisms for Low-Light Therapy III. doi:10.1117/12.764918
28. Yu, G. (2012). Near-infrared diffuse correlation spectroscopy in cancer diagnosis and therapy monitoring. *J. Biomed. Opt. Journal of Biomedical Optics, 17*(1), 010901. doi:10.1117/1.jbo.17.1.010901

29. Berne, B. J., & Pecora, R. (1990). Dynamic light scattering: With applications to chemistry, biology, and physics. Malabar, FL: Krieger.

30. Chu, B. (1991). Laser light scattering: Basic principles and practice. New York: Academic Press.

31. Brown, W. (1993). Dynamic Light Scattering: The Method and Some Applications. New York: Clarendon Press.

32. Boas, D. A., Pitris, C., & Ramanujam, N. (2011). Handbook of Biomedical Optics. Boca Raton: CRC Press.

33. Chao Z. (2007). *In-vivo Optical Imaging and Spectroscopy of Cerebral Hemodynamics* (Unpublished doctoral dissertation). University of Pennsylvania, Philadelphia, U.S.A.

34. http://www.ni.com/pdf/manuals/320999e.pdf.

35. http://sine.ni.com/nips/cds/print/p/lang/en/nid/1123.

36. Hase S. (2015). *Transcranial Near Infrared Spectroscopy and Stimulation of Prefontal Cognitive Functions in Young Adults.* University of Texas at Arlington, Texas, U.S.A.

37. http://www.mathworks.com/help/econ/autocorr.html

38. Sunar, U. *et al*. Noninvasive diffuse optical measurement of blood flow and blood oxygenation for monitoring radiation therapy in patients with head and neck tumors: a pilot study. *J. Biomed. Opt.* **11**, 064021 (2006).

39. Pogue, B. W. & Patterson, M. S. Review of tissue simulating phantoms for optical spectroscopy, imaging and dosimetry. *J. Biomed. Opt.* **11**, 041102 (2006).

40. He, L., Lin, Y., Shang, Y., Shelton, B. J., & Yu, G. (2013). Using optical fibers with different modes to improve the signal-to-noise ratio of diffuse correlation spectroscopy flow-oximeter measurements. J. Biomed. Opt Journal of Biomedical Optics, 18(3), 037001. doi:10.1117/1.jbo.18.3.037001

41. Barrett, D. & Gonzalez-Lima, F. Transcranial Infrared Laser Stimulation Produces Beneficial Cognitive And Emotional Effects In Humans. *Neuroscience* **230**, 13-23 (2013; 2012).

42. Hashmi, J. T. *et al*. Role of Low-Level Laser Therapy in Neurorehabilitation. *PM & R: the journal of injury, function, and rehabilitation* **2**, S292-S305 (2010).

43. Naeser, M. A., Saltmarche, A., Krengel, M. H., Hamblin, M. R. & Knight, J. A. Improved Cognitive Function After Transcranial, Light-Emitting Diode Treatments in Chronic, Traumatic Brain Injury: Two Case Reports. *PHOTOMEDICINE AND LASER SURGERY* **29**, 351-358 (2011).

44. Yu, K. G. (2013). Diffuse Correlation Spectroscopy (DCS) for Assessment of Tissue Blood Flow in Skeletal Muscle: Recent Progress. Anat Physiol Anatomy & Physiology, 03(02). doi:10.4172/2161-0940.1000128

45. Buckley, E. M., Parthasarathy, A. B., Grant, P. E., Yodh, A. G., & Franceschini, M. A. (2014). Diffuse correlation spectroscopy for measurement of cerebral blood flow: Future prospects. Neurophoton Neurophotonics, 1(1), 011009. doi:10.1117/1.nph.1.1.011009.

46. Rogatkin, D. A., & Dunaev, A. V. (2014). Stimulation of Blood Microcirculation at Low Level Laser Therapy: Monitoring Tools and Preliminary Data. Journal of Medical Research and Development (JMRD).

Biographical Information

Sagar Sunil Soni was born in Mumbai, India on June 4th 1992. He completed his Bachelors in Biomedical Engineering from University of Mumbai, India in June 2014. He worked as a Project Intern at AUM MEDITEC, India while doing his Bachelors towards development of a low-cost, wearable electrocardiograph. In Fall 2014, he began his graduate studies at University of Texas at Arlington. To pursue his passion for research he joined Dr. Hanli Liu's Biomedical Optics Lab. His research work during the course involved the development of a novel diagnostic modality, Diffused Correlation Spectroscopy and understanding the effects of laser stimulation. He plans to pursue his interests in medical device research and development by taking up related challenging projects in healthcare and allied fields.